Boletín de la Sociedad Geológica Mexicana
ISSN: 1405-3322
Sociedad Geológica Mexicana A.C.

Hernández-González, Juan S.; Butjosa, Lídia; Pujol-Solà, Núria; Aiglsperger, Thomas; Weber, Marion; Escayola, Mónica; Ramírez-Cárdenas, Carlos; Blanco-Quintero, Idael F.; González-Jiménez, José María; Proenza, Joaquín A.

Petrology and geochemistry of high-Al chromitites from the Medellín Metaharzburgitic Unit (MMU), Colombia

Boletín de la Sociedad Geológica Mexicana, vol. 72, no. 3, 00005, 2020
Sociedad Geológica Mexicana A.C.

DOI: https://doi.org/10.7440/res64.2018.03

Petrology and geochemistry of high-Al chromitites from the Medellín Metaharzburgitic Unit (MMU), Colombia

Petrología y geoquímica de cromititas ricas en Al de la Unidad Metaharzburgítica de Medellín (UMM), Colombia

Juan S. **Hernández-González**[1,2], Lídia **Butjosa**[1], Núria **Pujol-Solà**[1,*], Thomas **Aiglsperger**[3], Marion **Weber**[4], Mónica **Escayola**[5], Carlos **Ramírez-Cárdenas**[1], Idael F. **Blanco-Quintero**[6], José María **González-Jiménez**[7], Joaquín A. **Proenza**[1]

[1] Departament de Mineralogia, Petrologia i Geologia Aplicada, Facultat de Ciències de la Terra, Universitat de Barcelona, C/ Martí i Franquès s/n, 08028, Barcelona, Spain.

[2] Departamento de Mineralogia e Geotectônica, Instituto de Geociências (GMG-IGc), Universidade de São Paulo, Rua do Lago 562, 05508-080, São Paulo, Brazil.

[3] Department of Civil Engineering and Natural Resources, Division of Geosciences and Environmental Engineering, Luleå University of Technology, SE 97187, Luleå, Sweden.

[4] Departamento de Geociencias y Medio Ambiente, Facultad de Minas, Universidad Nacional de Colombia, Avenida 80 # 65-223, 050034, Medellín, Colombia.

[5] Instituto de Ciencias Polares y Ambientales ICPA, Universidad de Tierra del Fuego-CONICET, Fueguia Basket 251, 9410, Ushuaia, Tierra del Fuego, Argentina.

[6] Departamento de Ciencias de la Tierra y del Medio Ambiente, Universidad de Alicante, Carretera de San Vicente del Raspeig s/n, 03690, Alicante, Spain.

[7] Departamento de Mineralogía y Petrología, Facultad de Ciencias, Universidad de Granada, Avda. Fuentenueva s/n, 18002, Granada, Spain.

* Corresponding author: (N. Pujol-Solà)
npujolsola@ub.edu

How to cite this article:
Hernández-González, J.S., Butjosa, L., Pujol-Solà, N., Aiglsperger, T., Weber, M., Escayola, M., Ramírez-Cárdenas, C., Blanco-Quintero, I.F., González-Jiménez, J.M., Proenza, J.A., 2020, Petrology and geochemistry of high-Al chromitites from the Medellin Metaharzburgitic Unit (MMU), Colombia: Boletín de la Sociedad Geológica Mexicana, 72 (3), A120620. http://dx.doi.org/10.18268/BSGM2020v72n3a120620

Manuscript received: April 9,2020
Corrected manuscript received: June 11, 2020
Manuscript accepted: June 20, 2020

Peer Reviewing under the responsibility of Universidad Nacional Autónoma de México.

ABSTRACT

The Medellin Metaharzburgitic Unit (MMU), emplaced onto the western continental margin of Pangea during Triassic time, is located in the Central Cordillera of Colombia and consists of metaharzburgites, minor metadunites and chromitite bodies (Patio Bonito and San Pedro ore deposits). The ultramafic rocks contain relicts of mantle-derived olivine, chromian spinel and minor orthopyroxene, and a later metamorphic mineral assemblage composed by tremolite, chlorite, talc, fine-grained recrystallized olivine, serpentine-group minerals, magnetite, and secondary chromian spinel, formed during the thermal evolution of the unit. The Cr# [Cr/(Cr+Al) atomic ratio] of the accessory primary chromian spinel in the metaperidotites ranges from 0.58 to 0.62 and overlaps those of supra-subduction peridotites from ophiolites. According to textural and compositional variations, the accessory chromian spinel in the metaperidotites can be classified into three groups: i) partially altered chromian spinel with an Al-rich core, ii) porous, Cr-Fe^{2+}-enriched and Al-Mg-depleted chromian spinel, and iii) homogeneous Fe^{3+}-rich chromian spinel. These variations can be related to superimposed medium-T metamorphism that reached amphibolite facies (ca. 600 ºC). Chromitite bodies associated with the metaperidotites have massive and semi-massive textures, and mainly consist of chromian spinel crystals, which show large unaltered cores surrounded by thin alteration rims of ferrian chromian spinel and chlorite. Chromitites are Al-rich (#Cr <0.6) and strongly depleted in platinum group elements (ΣPGE <41 ppb). The primary petrological and geochemical characteristics preserved in the metaperidotites and chromitites indicate that the MMU formed at shallow levels of a suboceanic lithospheric mantle related to a supra-subduction zone (back-arc basin/incipient arc scenario), and that the chromitites crystallized from a tholeiitic magma (back-arc basin basalt type).

Keywords: Metaperidotite, chromian spinel, chromitite, ophiolite, supra-subduction zone, Colombia.

RESUMEN

La Unidad Metaharzburgítica de Medellín (UMM), emplazada en el margen continental de Pangea durante el Triásico, localizada en la Cordillera Central de Colombia, comprende metaharzburgitas y en menor proporción metadunitas y cuerpos de cromitita (depósitos de Patio Bonito y San Pedro). Estas rocas contienen olivino mantélico, Cr-espinela y en menor proporción ortopiroxeno, además de una asociación metamórfica posterior compuesta por tremolita, clorita, talco, olivino recristalizado de grano fino, minerales del grupo de la serpentina, magnetita y Cr-espinela secundaria, formada durante los procesos de evolución térmica de esta unidad. La Cr-espinela primaria tiene #Cr [Cr/(Cr+Al)] entre 0.58 y 0.62, similar a los valores de las peridotitas de zonas de suprasubducción. La Cr-espinela accesoria se puede clasificar en tres grupos según sus variaciones texturales y composicionales: i) Cr-espinela parcialmente alterada con un núcleo rico en Al, ii) Cr-espinela porosa, enriquecida en Cr-Fe^{2+} y empobrecida en Al-Mg, y iii) Cr-espinela homogénea rica en Fe^{3+}. Las variaciones texturales y composicionales de las Cr-espinelas accesorias son evidencia de un metamorfismo superpuesto que alcanzó facies anfibolita (ca. 600 ºC). Los cuerpos de cromitita asociados a las metaperidotitas tienen texturas masivas y semi-masivas y comprenden núcleos de Cr-espinela inalterada rodeados por bordes de Cr-espinela férrica y clorita. Las cromititas son ricas en Al (grado refractario: #Cr en la Cr-espinela primaria <0.6) y un contenido total muy bajo de elementos del grupo de platino (ΣPGE <41 ppb). Las características petrológicas y geoquímicas primarias de las metaperidotitas y las cromititas indican que estas últimas cristalizaron a partir de un magma toleítico (tipo basalto de cuenca de trasarco) y que la UMM representa niveles someros del manto litosférico suboceánico relacionado con una zona de suprasubducción (cuenca de trasarco/arco incipiente).

Palabras clave: Metaperidotita, Cr-espinela, cromitita, ofiolita, zona de suprasubducción, Colombia.

http://dx.doi.org/10.18268/BSGM2020v72n3a120620

1. Introduction

The Colombian Andes, located in the northwest of South America, are divided into three mountain ranges separated by valleys, namely from east to west: the Eastern Cordillera, the Magdalena River Valley, the Central Cordillera, the Cauca River Valley, and the Western Cordillera (Figure 1A). The western flank of the Central Cordillera, the Cauca River Valley, the Western Cordillera, and the Baudó Range make up the geographic region called "*Western Colombia*" (Restrepo and Toussaint, 1973; Bourgois *et al.*, 1987; Moreno-Sánchez and Pardo-Trujillo, 2003). Due to its high potential for precious metals, mainly gold, silver and Platinum-Group Elements (PGE), this region has been largely explored since pre-hispanic and colonial times.

Western Colombia is characterized by the occurrence of several ultramafic bodies (Figure 1A), some of them interpreted as: (1) fragments of an ophiolite mantle sequence (Restrepo and Toussaint, 1973; Álvarez, 1987; Bourgois *et al.*, 1987; Correa-Martínez, 2007) and (2) mantle portions of the Caribbean-Colombian oceanic plateau (Nivia, 1987; Kerr *et al.*, 1996; Serrano, 2009). The main ultramafic body of the Central Cordillera of Colombia is historically known as the Medellin Dunite (*e.g.*, Restrepo and Toussaint, 1984; Álvarez, 1987). It is located in the western flank of the Central Cordillera, northeast of Medellín (Department of Antioquia; Figure 1A) and is formed by peridotites metamorphosed at amphibolite facies conditions (ca. 600 °C, <6 kbar; Restrepo, 2008; García-Casco *et al.*, 2020 and references therein).

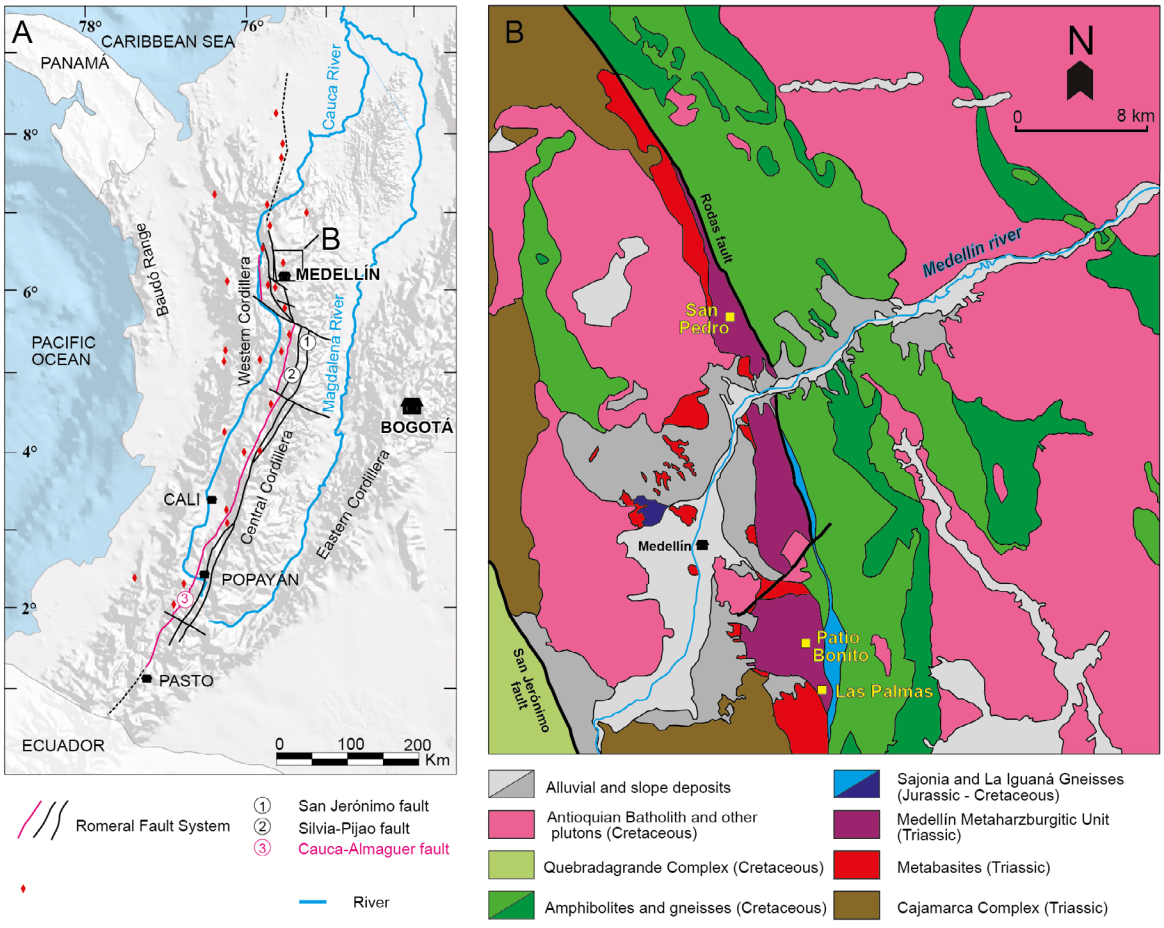

Figure 1 (A) Distribution map of peridotite bodies and mafic-ultramafic rock associations in Colombia (modified from Correa-Martínez, 2007; Gómez *et al.*, 2015). (B) Geological map of the Medellín region (modified from García-Casco *et al.*, 2020 and references therein). The location of the studied samples is shown in the map.

http://dx.doi.org/10.18268/BSGM2020v72n3a120620

This ultramafic body has been interpreted as the mantle section of the so-called Aburrá Ophiolite (Correa-Martínez, 2007). Using a bulk-rock major element geochemical approach, García-Casco *et al.* (2020) inferred that this ultramafic body is mainly harzburgitic, and that the term Medellin Metaharzburgitic Unit (MMU) is more appropriate than the historical "Medellin Dunite" term. The MMU hosts the best-known chromian spinel mineralization of Colombia, including the large deposit of Patio Bonito, located in the southern area of the ultramafic body (Figure 1B). This ore deposit contains refractory grade chromian spinel (Al-rich; Proenza *et al.*, 2004a; Correa-Martínez, 2007).

The origin of the MMU and its associated Cr-PGE mineralization has been a matter of debate for various decades (*e.g.*, Restrepo and Toussaint, 1973, 1984; Restrepo, 1986, 2008; Álvarez, 1987; Correa-Martínez and Nilson, 2003; Proenza *et al.*, 2004a; Pereira *et al.*, 2006; Correa-Martínez, 2007; García-Casco *et al.*, 2020 and references therein). Proenza *et al.* (2004a) and Correa-Martínez (2007) suggested that the MMU represents a fragment of oceanic lithospheric mantle formed in a supra-subduction environment. Pereira *et al.* (2006) documented a high PGE content in two samples of metadunite (up to 1.2 ppm), mainly of Pt, Pd, and Rh, suggesting a primary magmatic origin of the PGE content, chromian spinel and pentlandite. Accessory chromian spinel in ultramafic rocks provides valuable information about the petrogenesis of the host rock. Nevertheless, to date, there are no detailed studies of the textural and compositional characteristics of the accessory chromian spinel of the MMU, as well as its alteration.

This paper focuses on the study of the chromitite bodies hosted in the MMU. We have studied mineralogical, petrological and geochemical characteristics of chromitites and associated metaperidotites from Las Palmas, Patio Bonito and San Pedro, which cover the southern and northern sections of the ultramafic body (Figures 1B and 2).

2. Geological setting

2.1. MAFIC/ULTRAMAFIC ROCK ASSOCIATIONS IN THE COLOMBIAN ANDES

The central part of the Colombian Andes (Central Cordillera) comprises a metamorphic basement overlain by Mesozoic and Cenozoic sedimentary successions intruded by plutons of different ages, ranging from the Triassic to the Neogene (Feininger *et al.*, 1972; Vinasco *et al.*, 2006). In the western part of the Central Cordillera, there is an important tectonic boundary between Cretaceous oceanic crust to the west and the Paleozoic metamorphic continental basement to the east, called the Romeral Shear Zone (Figure 1A; Case *et al.*, 1971; McCourt *et al.*, 1984; Nivia, 1996; Vinasco, 2019). This complex shear zone consists of three main faults (from E to W): San Jerónimo, Silvia-Pijao and Cauca-Almaguer (Maya and González, 1995). The Cauca-Almaguer fault is considered to be the tectonic boundary between the Cretaceous rocks of oceanic affinity and the Paleozoic basement of the Central Cordillera (Nivia, 1996, 2001; Moreno-Sánchez and Pardo-Trujillo, 2003; López *et al.*, 2009). A series of mafic-ultramafic bodies of different ages lie on both sides of the Cauca-Almaguer fault (Figure 1A) (Restrepo and Toussaint, 1973; Bourgois *et al.*, 1987; Nivia, 1993; Moreno-Sánchez and Pardo-Trujillo, 2003).

The mafic-ultramafic bodies located to the west of the Cauca-Almaguer fault are associated with volcano-sedimentary rocks of oceanic affinity and are mainly considered to be fragments of a Cretaceous oceanic plateau (Nivia, 1987, 1996; Kerr *et al.*, 1996; Serrano, 2009). Nivia (1993) grouped these bodies into the Western Cretaceous Lithospheric Province. On the other hand, the majority of the mafic-ultramafic bodies and complexes located to the east of the Cauca-Almaguer fault are interpreted as of ophiolitic origin (Restrepo and Toussaint, 1973; Álvarez, 1987; Bourgois *et al.*, 1987; Correa-Martínez and Martens, 2000).

The Aburrá Ophiolite (Correa-Martínez, 2007; Figure 1B) is one of the mafic-ultramafic

http://dx.doi.org/10.18268/BSGM2020v72n3a120620

units that crops out to the east of the Cauca-Almaguer fault. It lies to the west of the low-grade metamorphic rocks of the Cajamarca Complex (Maya and González, 1995) that represents the paleo-continental margin. The Aburrá Ophiolite comprises ultramafic rocks that form the Medellin Metaharzburgitic Unit (MMU) and several mafic units, which include the El Picacho Metagabbros and the Espadera-Chupadero Amphibolites (Correa-Martínez and Martens, 2000; Correa-Martínez and Nilson, 2003; Correa-Martínez *et al.*, 2004, 2005; Correa-Martínez, 2007; Restrepo, 2008). The contacts between the different units of the Aburrá Ophiolite are tectonic and the MMU overthrusts the Espadera-Chupadero amphibolites (Figure 1B) (Restrepo and Toussaint, 1973; Rodríguez *et al.*, 2016).

2.2. MEDELLIN METAHARZBURGITIC UNIT (MMU)

The MMU covers approximately 71 km^2 and represents the main ultramafic body of ophiolitic affinity in the Colombian Central Cordillera (Figure 1B), which is in fault contact with Jurassic Sajonia mylontic gneisses and Cretaceous amphibolites (Figure 1B; Restrepo, 2008; Rodríguez *et al.*, 2016). This unit has been of special interest for chromium mining and exploration since it is a host for several small bodies of chromitite that were exploited over various decades (*e.g.*, Botero-Restrepo, 1945; Hall, *et al.*, 1970; Álvarez, 1987). Restrepo and Toussaint (1973) interpreted the ultramafic rocks of the MMU as part of an obducted ophiolite. Correa-Martínez and Nilson (2003) considered this unit to have formed in a subduction zone environment, and suggested that the origin of the MMU can be related to a Triassic back-arc basin. However, the age and the geodynamic setting of the ophiolite formation still remains a subject of debate (see Rodríguez *et al.*, 2016; Spikings and Paul, 2019; García-Casco *et al.*, 2020 and references therein). Correa-Martínez (2007) obtained an age of 216.6 ± 0.36 Ma (Late Triassic) in zircons from a plagiogranite dike intruding the El Picacho metagabbros, which was interpreted as the minimum age for the formation of the ophiolite oceanic crust. In addition, the age of emplacement of the Aburrá ophiolite onto the continent is still unknown, but a minimum pre-Cretaceous age is constrained by the intrusion of several apophysis of the Cretaceous Antioquia Batholith (Figure 1B) (Feininger and Botero, 1982; Correa-Martínez, 2007; Rodríguez *et al.*, 2016).

The MMU comprises mainly metaharzburgites and minor metadunites, containing tremolite, talc, chlorite, fine-grained recrystallized olivine, serpentine group minerals, magnetite, and chromian spinel, and to a lesser extent, carbonates, anthophyllite and relicts of magmatic olivine, chromian spinel and orthopyroxene (*e.g.*, Álvarez, 1987; Restrepo and Toussaint, 1984; Correa-Martínez, 2007; Restrepo, 2008), indicating medium-grade metamorphic conditions (ca. 600 °C). García-Casco *et al.* (2020) analyzed two possible geodynamic settings in order to explain the metamorphism of the MMU and associated metabasites: i) ocean-floor metamorphism (*e.g.*, Correa-Martínez, 2007), and ii) intra- back-arc subduction-initiation metamorphism, which supposes a new tectonic scenario for the MMU (García-Casco *et al.*, 2020).

2.3. THE CHROMITITE BODIES

Chromitite bodies occur mainly as centimetric to metric pods, but also as dikes, lenses, and disseminated schlieren (Álvarez, 1987), showing massive to disseminated textures. Chromitites usually show sharp contacts with the enclosing strongly serpentinized dunite (metadunite) and are concordant to subconcordant with the foliation of the host ultramafic rock (Correa-Martínez, 2007). The ore bodies are small, containing a maximum tonnage estimate of ~20000 tons of ore. They were exploited during the 1970's-1980's by metallurgical and glass industries (Correa-Martínez, 2007). The Patio Bonito deposit was the largest in the area, with 30 m length and up to 7 m width (Álvarez, 1987). Artisanal mining activity was reactivated in the 2000's with the opening of small mines and quarries in the northern and southern bodies (Correa-Martínez, 2007).

http://dx.doi.org/10.18268/BSGM2020v72n3a120620

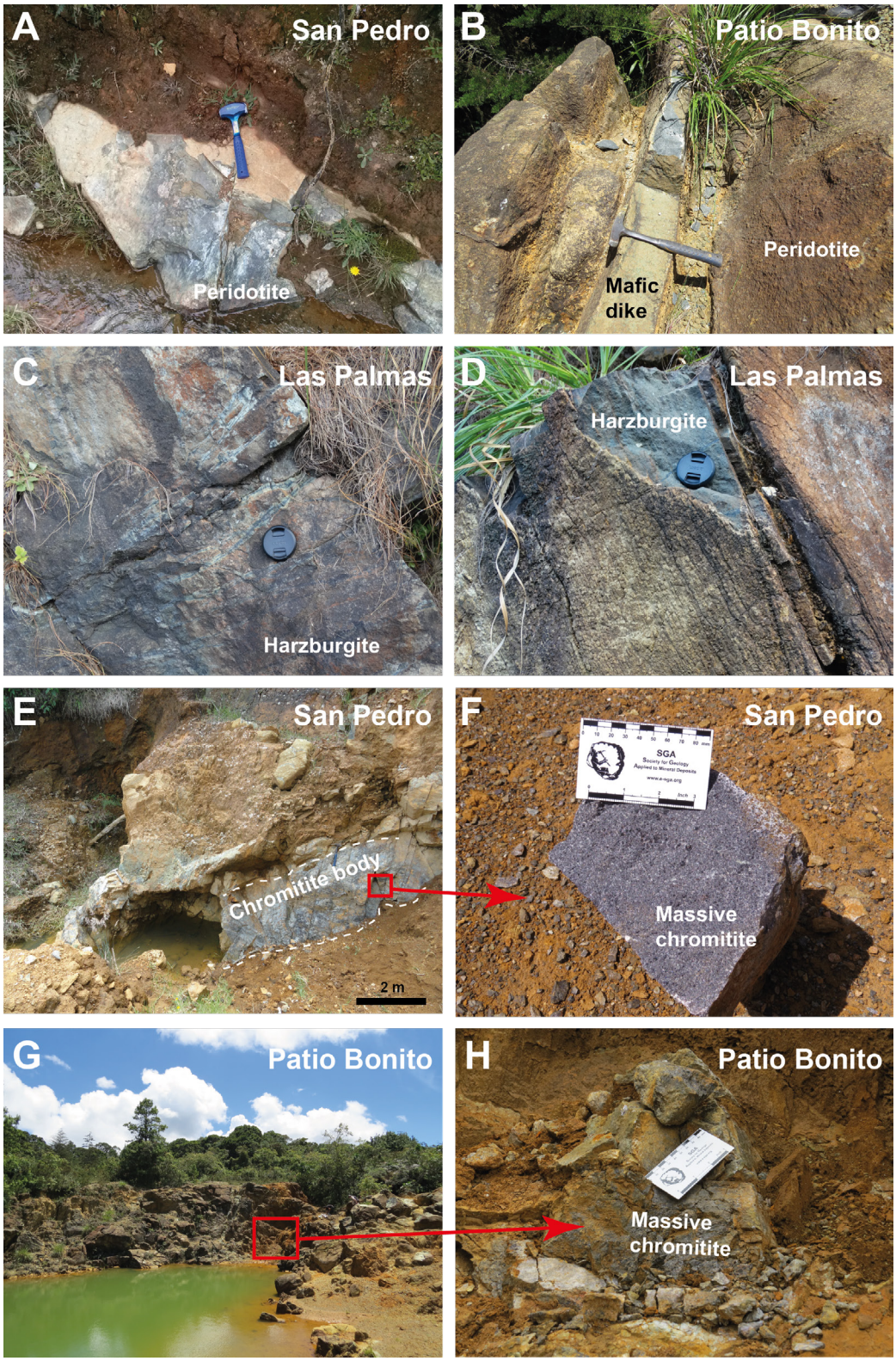

Figure 2 Field photographs of San Pedro, Patio Bonito, and Las Palmas localities. (A) Metaperidotite outcrop in the San Pedro locality. (B) Metaperidotite outcrop crosscut by a mafic dike or sill in the Patio Bonito locality. (C) and (D) Metaharzburgite outcrops in the Las Palmas locality. (E) Chromitite body in the San Pedro locality. (F) Massive chromitite hand-specimen from the San Pedro locality. (G) General view of the Patio Bonito Mine. (H) Zoom on the massive chromitite in the Patio Bonito locality.

http://dx.doi.org/10.18268/BSGM2020v72n3a120620

Table 1. Whole rock analyses of the Medellin Metaharzburgitic Unit (MMU) metaperidotites.

Sample	LP-1	LP-4	LP-7	SP-1
Locality	*Las Palmas*	*Las Palmas*	*Las Palmas*	*San Pedro*
Type of rock	*Metaharzburgite*	*Metaharzburgite*	*Metadunite*	*Metaharzburgite*
SiO_2 (wt%)	39.59	40.60	31.18	38.93
TiO_2	0.02	0.06	0.30	0.04
Al_2O_3	0.84	0.96	5.27	0.77
Fe_2O_{3T}	8.61	8.02	10.80	7.58
MnO	0.13	0.12	0.12	0.12
MgO	41.20	40.36	37.20	39.92
CaO	0.57	0.74	0.07	0.53
Na_2O	b.d.l.	b.d.l.	b.d.l.	b.d.l.
K_2O	b.d.l.	b.d.l.	b.d.l.	b.d.l.
P_2O_5	0.01	0.01	0.01	0.01
LOI	8.17	8.63	9.79	11.29
Total	99.14	99.50	94.74	99.19
Sample	LP-1	LP-4	LP-7	SP-1
Li (ppm)	1.1	0.9	2.3	1.5
Rb	0.80	0.37	0.38	0.60
Cs	0.071	0.008	0.037	0.027
Be	0.19	0.19	0.19	0.19
Sr	2.7	0.9	2.8	1.7
Ba	1.49	0.46	0.47	0.83
Sc	6.2	7.3	8.4	7.4
V	28.9	122.5	30.5	28.6
Cr	2231	12771	1488	1558
Co	101	129	98	109
Ni	2241	3593	1927	2260
Cu	1.3	113	2.6	19

b.d.l. = below detection limit.

3. Studied samples and analytical techniques

A total of 19 representative samples from Las Palmas, San Pedro and Patio Bonito outcrops (Figure 2) were selected to be studied on polished thin sections using optical microscopy (transmitted and reflected light). These include metaharzburgites and metadunites from Las Palmas, San Pedro and Patio Bonito also chromitites at San Pedro and Patio Bonito. The textural study of the chromian spinel alteration and the mineralogical characterization of the fine grain phases was carried out with Scanning Electron Microscopy with Energy-Dispersive X-Ray Spectroscopy (SEM-EDS) using the ESEM Quanta 200 FEI, XTE 325/D8395 at the Serveis Científics i Tecnològics (CCiTUB), Universitat de Barcelona. For the mineral chemistry analyses, the JEOL JXA-8230 electron microprobe was used at the same institution. Operating conditions were set to an acceleration voltage of 20 kV and a beam current of 20 nA. The elements were acquired using the analyzing crystals: LiF for Fe, Mn, and

http://dx.doi.org/10.18268/BSGM2020v72n3a120620

Table 1. (Continuation) Whole rock analyses of the Medellin Metaharzburgitic Unit (MMU) metaperidotites.

Sample	LP-1	LP-4	LP-7	SP-1
Locality	*Las Palmas*	*Las Palmas*	*Las Palmas*	*San Pedro*
Type of rock	*Metaharzburgite*	*Metadunite*	*Metaharzburgite*	*Metaharzburgite*
Zn	44	134	33	42
Ga	0.7	5.3	0.9	0.7
Yb	0.48	0.08	0.79	0.26
Nb	0.45	0.28	0.12	0.09
Ta	0.14	0.11	0.11	0.11
Zr (XRF)	8.8	5.8	5.6	7.0
Zr (ICPMS)	1.1	0.6	4.5	0.6
Mo	0.14	0.18	0.13	0.16
Sn	0.36	0.34	0.31	0.32
Tl	0.005	0.007	0.003	0.004
Pb	0.49	0.15	0.19	0.29
U	0.016	0.008	0.009	0.006
Th	0.203	0.054	0.041	0.024
La	0.084	0.043	0.080	0.056
Ce	0.174	0.078	0.239	0.098
Pr	0.027	0.011	0.039	0.014
Nd	0.143	0.031	0.183	0.072
Sm	0.047	0.007	0.085	0.020
Eu	0.019	0.002	0.016	0.006
Gd	0.052	0.007	0.088	0.019
Tb	0.008	0.001	0.017	0.004
Dy	0.063	0.007	0.124	0.027
Ho	0.013	0.002	0.026	0.009
Er	0.043	0.007	0.072	0.023
Tm	0.01	0.002	0.017	0.007
Yb	0.061	0.016	0.098	0.045
Lu	0.008	0.003	0.015	0.008
Hf	0.52	0.37	0.39	0.31

Ni; TAP for Mg and Al; PET for Cr, V, and Ti. The standards used were chromian spinel (Cr, Al, Fe), periclase (Mg), rhodonite (Mn), nickel oxide (Ni), rutile (Ti), metallic vanadium (V), albite (Na), wollastonite (Ca), and orthoclase (Si, K).

Whole rock analyses of peridotite samples were carried out in the Centro de Instrumentación Científica (CIC), Universidad de Granada. Major elements and Zr were analyzed using a Philips Magix Pro (PW-2440) X Ray Fluorescence (XRF). Trace elements abundances (except Zr) were obtained by ICP Mass Spectrometry (ICP-MS). Details of the analytic protocols have been described by Lázaro *et al.* (2014). Results are shown in Table 1. Platinum-Group Elements analyses were performed by ICP-MS method at

http://dx.doi.org/10.18268/BSGM2020v72n3a120620

Table 2. Whole rock platinum group elements (PGE) analyses of the MMU chromitites (ppb).

	San Pedro		Patio Bonito	
Sample	SP2	SP1	OF12	OF12A
Os	4	8	b.d.l.	b.d.l.
Ir	4	8	7	3
Ru	17	18	14	7
Rh	1	2	2	1
Pt	b.d.l.	3	4	3
Pd	2	2	b.d.l.	b.d.l.
ΣPGE	28	41	27	14

b.d.l. = below detection limit.

Genalysis Laboratory Services Pty. Ltd. in Maddington (Australia). The detection limits were 1 ppb for Rh and 2 ppb for Os, Ir, Ru, Pt, and Pd. The details of the analytical procedure can be found in Gervilla *et al.* (2005) and the results are shown in Table 2.

4. Results

4.1. PETROGRAPHY

4.1.1. ULTRAMAFIC ROCKS

The metaperidotite samples (Figure 2) correspond to metaharzburgites (>40% Ol and >5% Opx) and metadunites (>90% Ol), both partially serpentinized (Figures 3A to 3D). The preserved primary textures are typical of mantle tectonites, predominantly porphyroclastic/granoblastic textures, and minerals show undulose extinction and kink-bands. The ultramafic rocks contain relicts of mantle-derived olivine, chromian spinel, and minor orthopyroxene. However, much of the mineral assemblage is secondary and includes secondary fine-grained olivine, tremolite, chlorite, talc, serpentine, secondary chromian spinel, and minor carbonates and anthophyllite (García-Casco *et al.*, 2020 and references therein).

Metaharzburgites: Metaharzburgites show pseudomorphic mesh and bastite textures, where mantle olivine is replaced by serpentine and iddingsite along rims and fractures, and pyroxene by serpentine and tremolite (Figure 3A and 3B). There are two generations of olivine: primary olivine (Ol1), which forms 100-500 μm porphyroclasts, and secondary recrystallized olivine (Ol2) that forms smaller (< 20 μm) rounded grains (Figure 3B). Primary olivine is variably deformed and oriented, showing undulose extinction and kink-bands, and is also found as relict inclusions in pyroxene pseudomorphs. Non-pseudomorphic textures, characterized by intergrowths of antigorite, tremolite and secondary olivine are also observed (Figure 3A). Talc and chlorite replace mainly serpentine.

Chromian spinel (600-800 μm) is a common accessory phase in the MMU metaperidotites. Three types of chromian spinel can be distinguished petrographically, and can be classified according to the textural classification proposed by Gervilla *et al.* (2012): type I partially altered chromian spinel (Figures 4A and 4B), type II porous chromian spinel, which is completely altered and contains abundant chlorite within the porosity (Figures 4C and 4D), and type III homogeneous chromian spinel (Figures 4E and 4F). Both types I and II chromian spinel in the MMU are surrounded by a decussate chlorite corona.

Metadunites: Metadunites are less abundant than metaharzburgites in the MMU, and have been observed in Las Palmas and San Pedro localities (Figure 1B). In San Pedro, metadunites occur as envelopes around chromitite bodies. Metadunites show pseudomorphic mesh textures, where serpentine replaces primary olivine porphyroclasts along grain boundaries and fractures (Figure 3C). Primary mantle olivine forms crystals ~100 μm in size and secondary olivine forms smaller (~10 to 20 μm) crystals. Tremolite and talc are found as overgrowths in serpentine and filling thin veinlets (Figure 3C).

http://dx.doi.org/10.18268/BSGM2020v72n3a120620

Accessory chromian spinel (0.6 - 1 mm) shows unaltered cores surrounded by rims of porous chromian spinel with chlorite following the altered chromian spinel (111) crystallographic planes (Figure 4A and 4B). This partially altered chromian spinel corresponds to type I spinel according to the classification of Gervilla *et al.* (2012). A decussate chlorite corona surrounds the type II chromian spinel (Figure 3D). Chlorite crystals reach up to 500 µm in size and neither primary pyroxene nor pseudomorphs after pyroxene are observed.

4.1.2. CHROMITITES

Chromitite samples from San Pedro and Patio Bonito localities (Figures 3E to 3H) exhibit massive (>80% vol. chromian spinel) and semi-massive (60–80% vol. chromian spinel) textures. Massive chromitites consists of large (0.5-0.8 cm) chromian spinel crystal aggregates, which have unaltered cores surrounded by thin alteration rims of ferrian chromian spinel with abundant chlorite inclusions (Figure 3G), also showing typical pull-apart textures. Semi-massive chromitites are made up of smaller chromian spinel grains (up to 0.2 cm) that are strongly fractured and altered along rims to ferrian chromian spinel (Figure 3H), locally forming brecciated textures. Chlorite is the predominant intergranular mineral accompanied by minor serpentine, rutile, ilmenite, and titanite. Mineral inclusions observed within chromian spinel include olivine, chlorite, serpentine, ilmenite, rutile, and amphibole. In both chromitite bodies, chromian spinel alteration rims are highly porous and the voids are filled by chlorite and minor sulfides. The voids within the alteration rims in the less altered chromian spinel crystals are rounded (Figure 3H), whereas the ones in the more altered crystals have coarse irregular or acicular-shaped voids (Figures 4A to 4D).

4.2. WHOLE ROCK GEOCHEMISTRY

4.2.1. METAPERIDOTITES

The LOI values of the MMU metaperidotites range from 8.17 to 11.29 wt% (Table 1). The Al_2O_3 contents (0.84 - 0.96 wt%) are rather low (except for sample LP-7), SiO_2 ranges between 31.18 and 40.60 wt%, Fe_2O_3 between 7.58 and 10.80 wt%, MgO between 37.20 to 41.20 wt%, and CaO and TiO_2 contents are low (0.07 - 0.74 wt% and 0.02 - 0.30 wt% respectively) (Table 1). One metadunite from Las Palmas (sample LP-7) shows the lowest contents of SiO_2 and CaO (31.18 wt% and 0.07 wt% respectively), and the highest contents of TiO_2 (0.30 wt%), Al_2O_3 (5.27 wt%), and Fe_2O_3 (10.80 wt%) (Table 1).

Chondrite-normalized rare earth element (REE) patterns (Figure 5A) are almost flat or U-shaped. The metaharzburgite sample from San Pedro (SP-1) shows a positive Ho anomaly and a negative Er anomaly. One metaharzburgite sample from Las Palmas (LP-4) is clearly depleted in REEs when compared to the other samples. The metadunite (LP-7), which is already particular in terms of major elements, shows a noticeable negative Eu anomaly, not observed in the other samples.

In the multielemental diagram normalized to the primitive mantle (Figure 5B) metaperidotites are typically depleted in large-ion lithophile elements (LILE) and slightly enriched in high field strength elements (HFSE). All samples show positive Th and Pb anomalies.

4.2.2. CHROMITITES: PGE GEOCHEMISTRY

Whole rock PGE contents normalized to chondritic values for the massive chromitites associated with the MMU (Figure 6) show a general PGE depletion, around 100 times lower than chondritic values. The San Pedro chromitites have ΣPGE < 41 ppb, Ru being the most abundant element (17 - 18 ppb). The Patio Bonito chromitites have ΣPGE < 37 ppb, Ru also being the most abundant element (7 - 14 ppb), but with a significantly lower content than in San Pedro. The chondrite-normalized PGE patterns (Figure 6) are characterized by comparable Os and Ir values, positive Ru anomalies, and a negative slope from Ru to Pd, which is typical for podiform chromitites (*e.g.*, Leblanc, 1991). These patterns are similar to those from the Al-rich chromitites from Tehuitzingo, México (Proenza *et al.*, 2004b).

http://dx.doi.org/10.18268/BSGM2020v72n3a120620

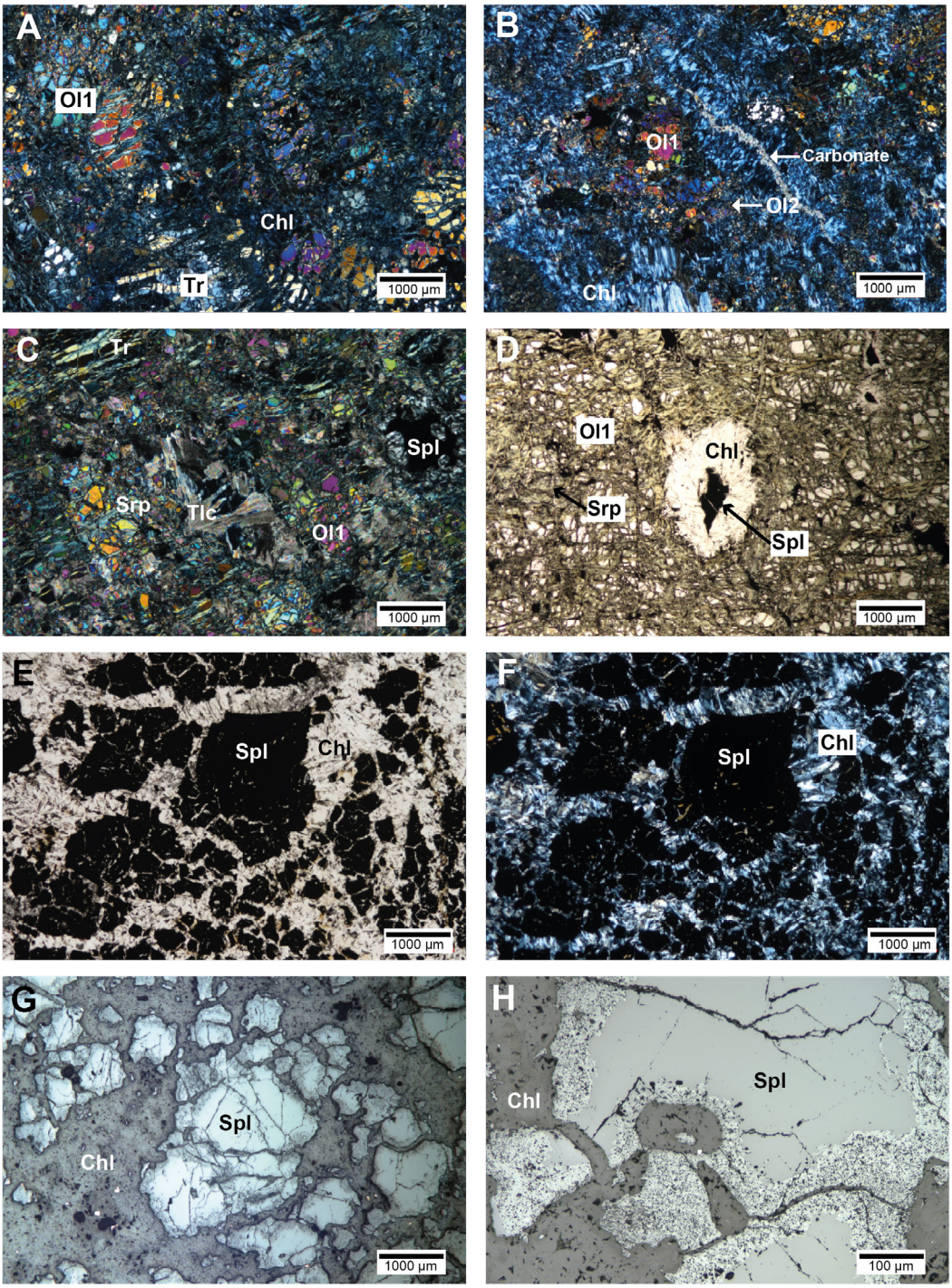

Figure 3 Microphotographs of metaharzburgites, metadunites and chromitites from the MMU. (A) Metaharzburgite with tremolite (*Tr*) and relict olivine (*Ol1*) replaced by serpentine and chlorite (*Chl*). Transmitted light and crossed nicols. (B) Metaharzburgite with relict olivine (*Ol1*), secondary olivine (*Ol2*), chlorite (*Chl*) and late carbonate veins. Transmitted light and crossed nicols. (C) Metadunite showing magmatic olivine (*Ol1*) altered to serpentine (*Srp*) and iddingsite. Talc (*Tlc*) and accessory spinel (*Spl*) are also observed. Transmitted light and crossed nicols. (D) Metadunite with olivine (*Ol1*) partially altered to serpentine. Chromian spinel (*Spl*) is surrounded by a decussate chlorite (*Chl*) corona. Transmitted light and parallel nicols. (E) Chromitite with coarse chromian spinel (*Spl*) crystals in a chlorite matrix (*Chl*). Transmitted light and parallel nicols. (F) Same as E in transmitted light and crossed nicols. (G) Chromitite showing strongly altered and fractured chromian spinel (*Spl*) crystals surrounded by chlorite (*Chl*). Reflected light. (H) Chromitite showing alteration rims in chromian spinel (*Spl*) crystals in chromitite. Reflected light.

http://dx.doi.org/10.18268/BSGM2020v72n3a120620

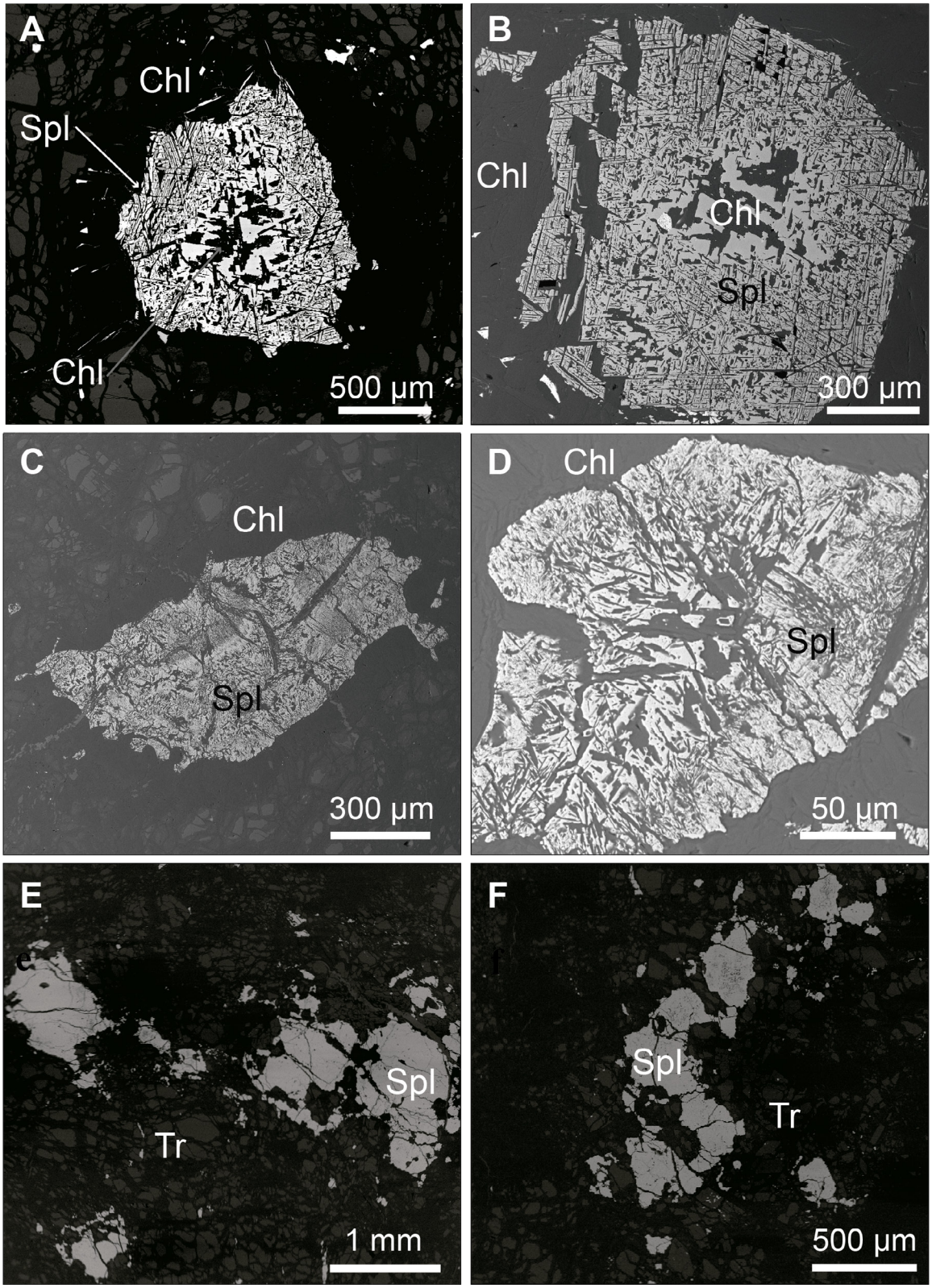

Figure 4 Back-scattered electron images (BSE) of the accessory chromian spinel in MMU. (A) and (B) Type I chromian spinel (*Spl*) (Al-rich) in metaperidotite. Chlorite (*Chl*) is present as inclusions within the chromian spinel that follow the (111) crystallographic planes and as a corona surrounding the spinel. (C) and (D) Type II chromian spinel (Cr-Fe^{2+}-rich, and Al-Mg-depleted) with chlorite inclusions and a chlorite halo surrounding the spinel. (E) and (F) Type III chromian spinel (Fe^{3+}-rich) intergrown with tremolite (*Tr*).

http://dx.doi.org/10.18268/BSGM2020v72n3a120620

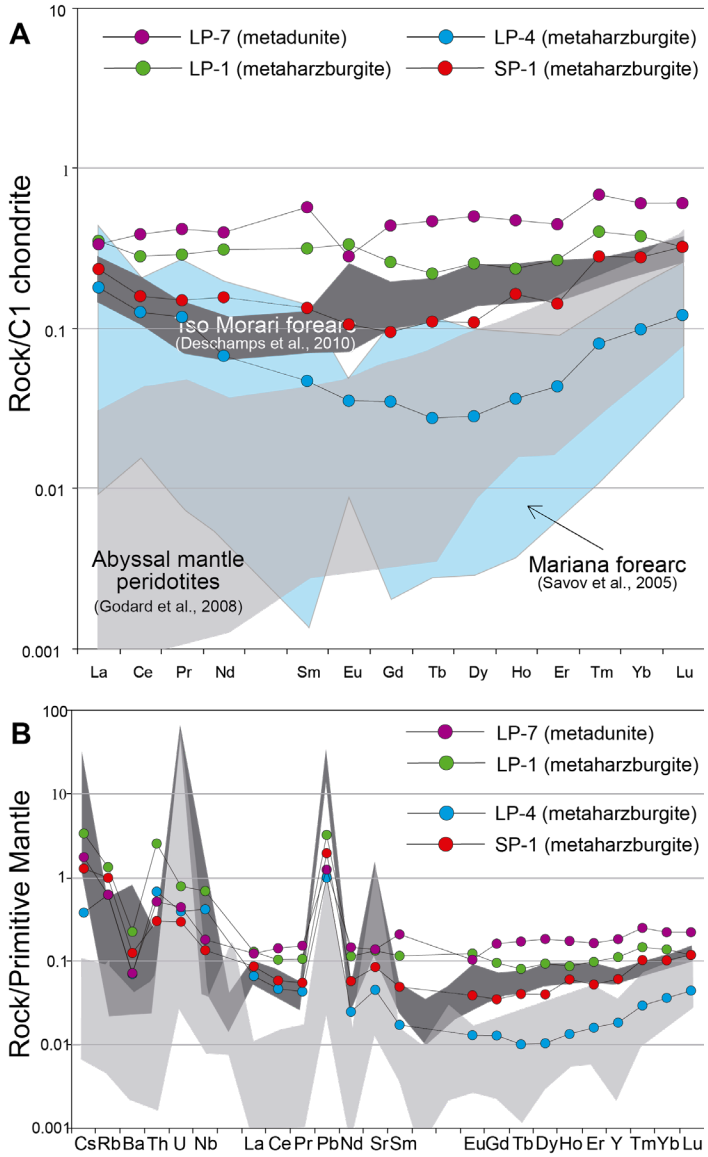

Figure 5 Whole rock geochemistry of the Las Palmas (LP-1, LP-4 and LP-7) and San Pedro (SP-1) metaperidotites. (A) Chondrite-normalized REE patterns. (B) Multi-elemental diagram normalized to the primitive mantle. The fields for abyssal mantle peridotites (Godard *et al.*, 2008) and hydrated mantle wedge serpentinites (Tso Morari, Himalaya, Deschamps *et al.*, 2010; Mariana Forearc, Savov *et al.*, 2005) are projected for comparison. Normalizing values were taken from McDonough and Sun (1995).

4.3. MINERAL CHEMISTRY

4.3.1. CHROMIAN SPINEL

Accessory chromian spinel in the metaperidotites has been divided into 3 textural groups. The compositional variations regarding the Fe^{3+}, Cr and Al contents are directly related to the textural classification defined petrographically (Figures 7A, 7B,8 and Table 3).

- Type I chromian spinel (partially altered) has Al-rich cores (Figures 7A and 8A, Table 3) that represent the primary composition. These cores are characterized by Cr# [Cr/(Cr+Al) atomic ratio] ranging from 0.58 to 0.62, Mg# [Mg/(Mg+Al) atomic ratio] from 0.42 to 0.44, Fe^{3+}# [Fe^{3+}/(Fe^{3+}+Cr+Al) atomic ratio] ≤ 0.03, TiO_2 ≤ 0.36 wt%, MnO from 0.32 to 0.42 wt%, and ZnO from 0.68 to 0.87 wt%. This composition is typical of accessory spinel in mantle rocks at supra-subduction zones (Kamenetsky *et al.*, 2001) (Figure 7A).
- Type II chromian spinel (porous) is Al and Mg-depleted and enriched in Cr, Fe^{2+}, Ti and Mn, when compared to Type I chromian spinel. The composition is characterized by Cr# that ranges from 0.84 to 0.96, Mg# from 0.13 to

http://dx.doi.org/10.18268/BSGM2020v72n3a120620

0.27, Fe^{3+}# from 0.05 to 0.16, TiO_2 from 0.42 to 1.57 wt%, MnO from 0.39 to 0.76 wt%, and ZnO from 0.37 to 0.66 wt% (Figure 7B, Table 3).

- Type III chromian spinel (homogenous) is Fe^{3+}-rich (Figures 7B and 8B, Table 3) and has Cr# that ranges from 0.98 to 1.00, Mg# from 0.09 to 0.22, Fe^3# from 0.30 to 0.79, TiO_2 from 0.27 to 0.45 wt%, MnO from 0.16 to 0.58 wt%, and ZnO from 0.04 to 0.28 wt%.

Unaltered chromian spinel cores from San Pedro chromitites has Cr# ranging from 0.43 to 0.58, Mg# from 0.54 to 0.68, TiO_2 from 0.02 to 0.5 wt%, Fe^{3+}# <0.035, MnO < 0.27 wt%, V_2O_3 < 0.22 wt%, ZnO < 0.17 wt%, and NiO < 0.23 wt% (Figures 7C, 7D, Table 4). In contrast, unaltered chromian spinel cores from Patio Bonito chromitites exhibit higher Cr# (0.51 - 0.63) and Mg# (0.67-0.80), similar TiO_2 (0.05 to 0.5 wt%) and NiO (<0.21 wt%) but lower Fe^3+# (<0.018 wt%) and slightly higher MnO (0.11-0.49 wt%), V_2O_3 (<0.26 wt%), and ZnO (<0.37 wt%) (Figures 7C, 7D and Table 4).

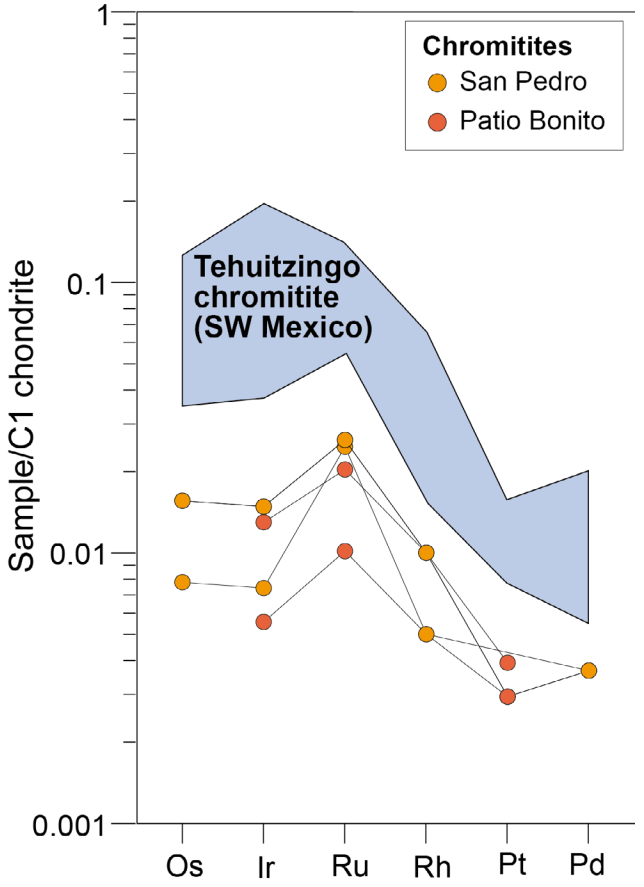

Figure 6 Chondrite-normalized platinum group element (PGE) patterns for the San Pedro and Patio Bonito chromitites. Normalizing chondritic values are from Naldrett and Duke (1980). The field for the Tehuitzingo chromitites (México) is from Proenza *et al.* (2004b).

4.3.2. OLIVINE

Olivine is only present in the metaperidotites and its composition ranges from $Fo_{89.7}$ to $Fo_{93.7}$ (average of $Fo_{90.5}$), and NiO from 0.19 to 0.51 wt%, which is within the range of mantle olivine (*e.g.*, Takahashi *et al.*, 1987). Even though petrographically it was possible to distinguish primary mantle-derived olivine and secondary metamorphic olivine, all the analyzed crystals show similar composition (Table 5). Figure 9A shows a scattering of olivine compositions between the abyssal peridotites (Moghadam *et al.*, 2015) and the supra-subduction peridotite fields (Ishii *et al.*, 1992).

4.3.3. TREMOLITE

Amphibole is only present in the metaharzburgites and it is more abundant in samples that contain Type-III chromian spinel. The studied crystals belong to the calcium subgroup (calculations following Locock, 2014) according to the classification scheme of Hawthorne *et al.* (2012), and have Mg# [Mg/(Mg+Fe^{2+}) atomic ratio] ranging from 0.95 to 0.99 (Table 6). These calcium amphiboles (Ca^B = 1.196 - 2 a.p.f.u; Na^B = 0.001 - 0.19) classify as tremolite (Figure 9B). Analyses yielded very low Ti (<0.02 a.p.f.u.), Mn (<0.06 a.p.f.u.) and K (<0.007 a.p.f.u.) contents, and have variable Si (7.20 - 8.02), Al^{TOT} (0.016 - 0.131), Mg (3.76 - 4.96), Fe^{TOT} (0.14 - 0.39), Ca (1.19 - 2.00), and Na (0.001 - 0.19) contents (Table 6). The vacancy in position A is between 0.69 and 1.00 a.p.f.u.

4.3.4. CHLORITE

Chlorite composition in the metaharzburgites corresponds to clinochlore and high-Si pennantite (Figure 9C) according to the classification by Hey (1954). SiO_2 content ranges from 27.91 to 35.21 wt% (up to 6.7 Si a.p.f.u.) and FeO from 1.79 to 3.37 wt% (up to 0.49 Fe^{2+} a.p.f.u.). The Fe/(Fe +

http://dx.doi.org/10.18268/BSGM2020v72n3a120620

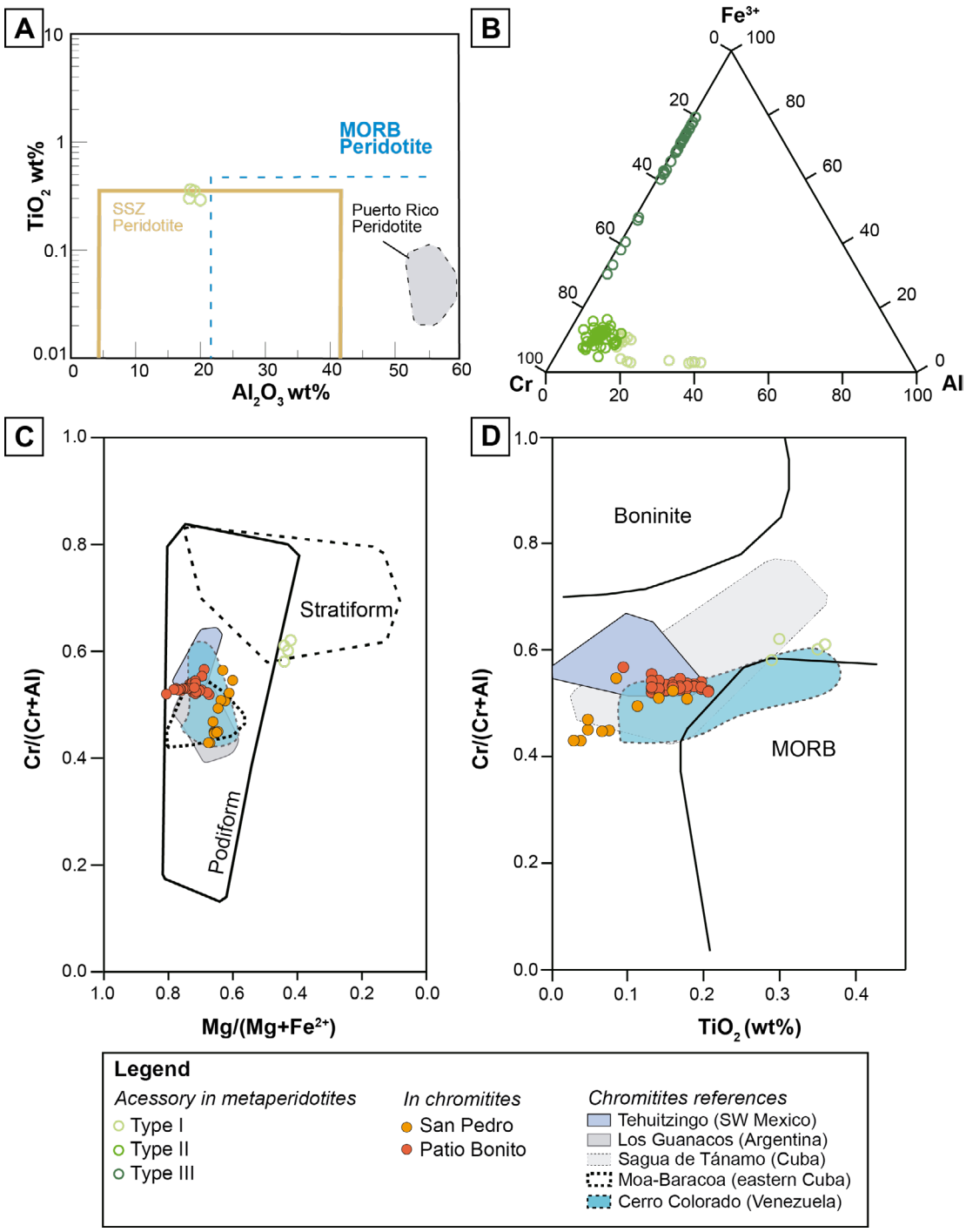

Figure 7 Mineral chemistry of accessory chromian spinel in the metaperidotites and in the chromitite bodies of the MMU. (A) TiO_2 (wt%) vs. Al_2O_3 (wt%) diagram for type I chromian spinel. Fields for supra-subduction zone (SSZ) and MORB-type peridotites are from Kamenetsky *et al.* (2001), and the field for the Puerto Rico Peridotite is from Marchesi *et al.* (2011). (B) Cr, Fe^{3+} and Al compositions for chromian spinel of the MMU. (C) Cr# [Cr/(Cr+Al)] vs. Mg# [Mg/(Mg+Fe)] diagram for chromian spinel of the San Pedro and Patio Bonito chromitites, and primary chromian spinel for the metaperidotites. The podiform and stratiform fields are after Irvine (1967) and Leblanc and Nicolas (1992) respectively, the Moa Baracoa and Sagua de Tánamo (Cuba) fields are from Proenza *et al.* (1999), Tehuitzingo (México) is from Proenza *et al.* (2004b), Los Guanacos (Argentina) is from Proenza *et al.* (2008), and Cerro Colorado (Venezuela) is from Mendi *et al.* (2020). (D) Cr# vs. TiO_2 (wt%) for the San Pedro and Patio Bonito chromitites, and type I chromian spinel in the metaperidotites. Fields for boninites and MORB are from Arai (1992), references are the same as in (C).

http://dx.doi.org/10.18268/BSGM2020v72n3a120620

Table 3. Representative electron microprobe analyses of accessory chromian spinel in the metaperidotites.

	Type I			Type II			Type III		
Area	*Las Palmas*	*Las Palmas*	*Las Palmas*	*Las Palmas*	*Las Palmas*	*San Pedro*	*Patio Bonito*	*Patio Bonito*	*Patio Bonito*
Sample	*LP-7*	*LP-7*	*LP-7*	*LP-7*	*LP-7*	*SP-001*	*COL-6*	*COL-7*	*COL-6*
SiO_2 (wt.%)	0.05	b.d.l.	0.07	b.d.l.	0.10	0.07	0.08	0.08	0.05
TiO_2	0.29	0.35	0.30	0.78	0.88	1.13	0.29	0.31	0.29
Al_2O_3	19.97	19.03	18.29	6.82	3.67	2.19	0.24	0.10	b.d.l.
Cr_2O_3	41.91	42.76	44.09	52.42	54.54	53.73	28.67	17.49	11.03
V_2O_3	0.16	0.17	0.14	0.25	0.33	0.33	0.16	0.16	0.11
Fe_2O_3	5.37	5.77	5.26	-	-	-	39.22	50.72	56.79
FeO	21.44	21.54	21.86	32.69	34.88	38.16	27.40	28.17	28.92
MnO	0.34	0.36	0.32	0.58	0.62	0.70	0.58	0.32	0.26
ZnO	0.87	0.68	0.79	0.50	0.57	0.63	0.24	0.07	0.08
MgO	8.44	8.39	8.10	5.08	3.54	2.55	2.19	1.81	1.18
NiO	0.12	0.05	0.05	0.04	b.d.l.	0.09	0.48	0.66	0.81
Total	98.96	99.11	99.27	99.15	99.14	99.58	99.55	99.89	99.52
	Type I			**Type II**			**Type III**		
Ti (a.p.f.u.)	0.01	0.01	0.01	0.02	0.02	0.03	0.01	0.02	0.02
Al	0.80	0.76	0.73	0.28	0.15	0.09	0.02	0.01	0.00
Cr	1.12	1.15	1.19	1.44	1.54	1.53	1.34	1.00	0.73
V	0.00	0.00	0.00	0.01	0.01	0.01	0.01	0.01	0.01
Fe^{3+}	0.06	0.06	0.05	0.24	0.24	0.31	0.60	0.94	1.22
Fe^{2+}	0.55	0.55	0.57	0.72	0.80	0.84	0.76	0.77	0.80
Mn	0.01	0.01	0.01	0.02	0.02	0.02	0.03	0.02	0.02
Zn	0.02	0.02	0.02	0.01	0.02	0.02	0.01	0.00	0.00
Mg	0.43	0.43	0.41	0.26	0.19	0.14	0.19	0.20	0.15
Ni	0.00	0.00	0.00	0.00	-	0.00	0.02	0.04	0.05
	Type I			**Type II**			**Type III**		
Cr#	0.58	0.60	0.62	0.84	0.91	0.94	0.99	0.99	1.00
Mg#	0.44	0.43	0.42	0.27	0.19	0.14	0.20	0.20	0.16
Fe^{3+}#	0.03	0.03	0.03	0.12	0.12	0.16	0.30	0.48	0.63

b.d.l. = below detection limit.

Mg) ratio ranges between 0.03 and 0.05, also the Cr_2O_3 content is low (<3.2 wt%) (Table 6).

Chlorite in the chromitites corresponds to clinochlore (Figure 9C), with SiO_2 ranging from 27.07 to 32.61 wt%, FeO from 1.22 to 1.79 wt% and Fe/(Fe + Mg) ratio between 0.02 and 0.03. These values are lower than those from chlorite found in metaperidotites. The Cr_2O_3 content is also low (<2.61 wt%).

4.3.5. SERPENTINE

Serpentine composition (Figure 9D) ranges from 41.54 to 45.98 wt% of SiO_2, FeO from 2.85 to 4.51 wt%, Al_2O_3 from 0.53 to 2.50 wt%, and Cr_2O_3 from 0.03 to 0.47 wt% (Table 6). The highest SiO_2 values are observed in serpentine from metaperidotites with type III accessory chromian spinel, where chlorite is rare.

http://dx.doi.org/10.18268/BSGM2020v72n3a120620

Table 4. Representative electron microprobe chromian spinel analyses from the chromitite bodies in the MMU.

Locality	San Pedro					Patio Bonito				
	chr1	chr2	chr3	chr4	chr5	chr1	chr2	chr3	chr4	chr5
SiO_2 (wt.%)	0.09	0.03	0.07	0.03	0.06	0.14	0.09	0.08	0.10	0.10
TiO_2	0.03	0.04	0.05	0.07	0.08	0.14	0.22	0.15	0.16	0.18
Al_2O_3	32.74	32.49	31.33	31.31	31.23	27.06	26.81	26.63	26.58	26.49
Cr_2O_3	36.56	36.28	38.01	37.53	37.71	43.38	43.21	43.03	43.37	43.99
V_2O_3	0.09	0.13	0.19	0.10	0.19	0.12	0.11	0.15	0.21	0.14
Fe_2O_3	2.07	2.63	1.87	2.15	2.26	0.82	3.13	2.64	0.95	1.85
FeO	13.40	13.54	13.92	13.89	14.02	13.11	8.65	11.98	12.89	9.74
MnO	0.14	0.20	0.19	0.16	0.18	0.17	0.11	0.20	0.19	0.13
ZnO	0.00	0.02	0.05	0.15	0.08	b.d.l.	0.05	0.07	0.12	0.11
MgO	15.70	15.51	15.13	15.05	15.09	15.10	18.16	15.93	15.07	17.25
NiO	0.08	b.d.l.	0.11	0.02	0.05	0.16	0.14	0.14	0.18	0.20
Total	100.89	100.89	100.94	100.47	100.93	100.20	100.68	101.00	99.82	100.18
	chr1	chr2	chr3	chr4	chr5	chr1	chr2	chr3	chr4	chr5
Ti (a.p.f.u.)	0.00	0.00	0.00	0.00	0.00	0.00	0.00	0.00	0.00	0.00
Al	1.11	1.11	1.07	1.08	1.07	0.95	0.94	0.94	0.94	0.93
Cr	0.83	0.83	0.87	0.87	0.87	1.03	1.02	1.02	1.03	1.04
V	0.00	0.00	0.00	0.00	0.00	0.00	0.00	0.00	0.01	0.00
Fe^{3+}	0.05	0.06	0.04	0.05	0.05	0.00	0.02	0.02	0.01	0.01
Fe^{2+}	0.32	0.33	0.34	0.34	0.34	0.33	0.19	0.28	0.32	0.23
Mn	0.00	0.01	0.01	0.00	0.00	0.00	0.00	0.01	0.00	0.00
Mg	0.68	0.67	0.66	0.66	0.66	0.67	0.81	0.71	0.68	0.77
Ni	0.00	-	0.00	0.00	0.00	0.00	0.00	0.00	0.00	0.00
	chr1	chr2	chr3	chr4	chr5	chr1	chr2	chr3	chr4	chr5
Cr#	0.43	0.43	0.45	0.45	0.45	0.52	0.52	0.52	0.52	0.53
Mg#	0.68	0.67	0.66	0.66	0.66	0.67	0.81	0.72	0.68	0.77
Fe^{3+}#	0.13	0.15	0.11	0.12	0.13	0.05	0.25	0.17	0.06	0.15

b.d.l. = below detection limit.

5. Discussion

5.1. TECTONIC SETTING OF THE MMU PERIDOTITES

Ophiolitic peridotites are spatially and temporally related with first-order tectonic and magmatic global events, which, together with mantle processes, control the development of different types of oceanic lithosphere ("ophiolites") in various tectonic settings (Dilek and Flower, 2003; Dilek and Furnes, 2014 and references therein). In general, oceanic ultramafic rocks of ophiolitic affinity can be classified as: (i) subduction zone (supra-subduction zone or volcanic arc) related ophiolites, which might be influenced by the dehydration of the subducting plate, associated metasomatic processes, and repetitive episodes of partial melting of metasomatized peridotites, and (ii) subduction unrelated ophiolites (oceanic ridges, MOR or plumes), which are linked to mantle diapirism, heat advection and melting in the asthenospheric mantle and/or at deeper levels.

http://dx.doi.org/10.18268/BSGM2020v72n3a120620

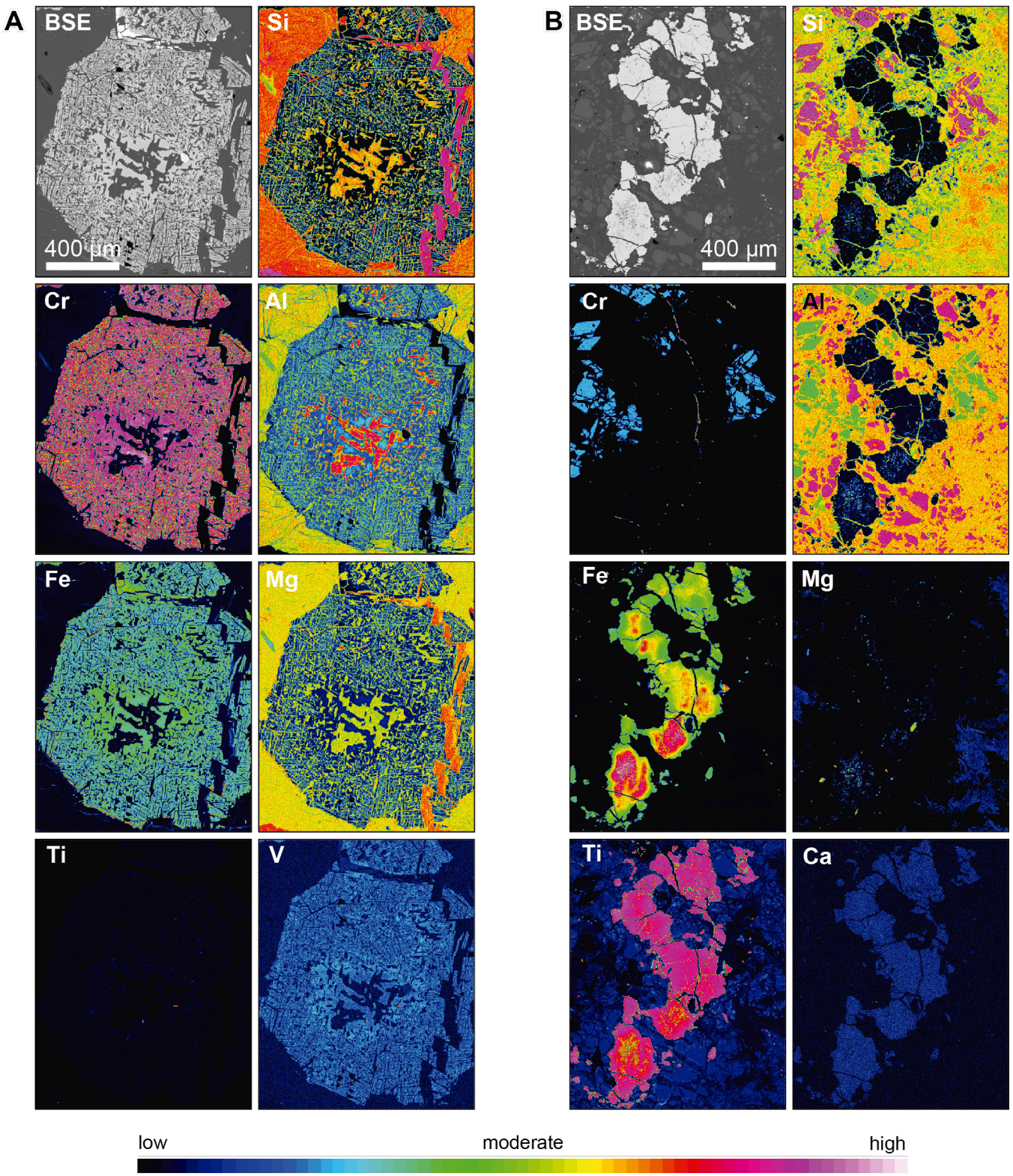

Figure 8 Element distribution maps for accessory chromian spinel in the MMU. (A) Type I chromian spinel from Las Palmas (Sample LP-7). Note the high Al, Fe, and Cr contents in the core that gradually decreases towards the rims. The Al-rich cores are surrounded by a high-V halo. (B) Type III chromian spinel from the Las Palmas metaperidotite (Sample CO-7). The Fe enrichment is related with the Cr depletion, whereas Al is almost absent.

http://dx.doi.org/10.18268/BSGM2020v72n3a120620

Table 5. Representative electron microprobe analyses of olivine in the metaperidotites.

Mineral	Ol-1	Ol-1	Ol-1	Ol-1	Ol-2	Ol-2	Ol-2	Ol-1	Ol-1	Ol-2	Ol-2	Ol-1	Ol-1	Ol-2	Ol-2	Ol-1	Ol-1	Ol-1	Ol-2	Ol-2	Ol-1	Ol-2	Ol-2	Ol-2	Ol-2
Locality	*Las Palmas*													*San Pedro*							*Patio Bonito*				
Type of rock	*dun*	*dun*	*dun*	*dun*	*dun*	*dun*	*dun*	*dun*	*dun*	*dun*	*dun*	*dun*	*dun*	*per*	*per*	*per*	*per*	*per*	*per*	*per*	*dun*	*dun*	*dun*	*dun*	*dun*
Sample	*LP-1*	*LP-1*	*LP-1*	*LP-1*	*LP-1*	*LP-1*	*LP-1*	*LP-7*	*LP-7*	*LP-7*	*LP-7*	*LP-7*	*LP-7*	*SP-1*	*SP-1*	*SP-1*	*SP-1*	*SP-1*	*SP-1*	*SP-1*	*CO-7*	*CO-7*	*CO-7*	*CO-7*	*CO-7*
SiO_2 (wt.%)	40.72	40.87	41.30	40.86	41.03	41.04	41.14	41.45	41.21	40.91	40.96	40.98	40.72	41.04	40.60	41.08	40.97	40.89	40.94	40.79	41.39	40.94	41.07	41.21	40.96
TiO_2	b.d.l.	0.04	b.d.l.	0.02	b.d.l.	0.02	b.d.l.	b.d.l.	b.d.l.	b.d.l.	b.d.l.	0.04	b.d.l.	0.02	b.d.l.	b.d.l.	0.03	0.02	b.d.l.	b.d.l.	0.02	0.03	b.d.l.	b.d.l.	0.05
Al_2O_3	b.d.l.	b.d.l.	b.d.l.	b.d.l.	b.d.l.	b.d.l.	b.d.l.	b.d.l.	b.d.l.	b.d.l.	b.d.l.	b.d.l.	b.d.l.	b.d.l.	b.d.l.	b.d.l.	b.d.l.	b.d.l.	b.d.l.	b.d.l.	b.d.l.	b.d.l.	b.d.l.	b.d.l.	b.d.l.
Cr_2O_3	0.03	b.d.l.	b.d.l.	b.d.l.	b.d.l.	b.d.l.	b.d.l.	0.02	0.02	b.d.l.	0.02	b.d.l.	b.d.l.	0.02	b.d.l.	b.d.l.	b.d.l.	b.d.l.	b.d.l.	b.d.l.	b.d.l.	b.d.l.	0.02	b.d.l.	0.02
V_2O_3	b.d.l.	0.02	b.d.l.	b.d.l.	b.d.l.	b.d.l.	b.d.l.	b.d.l.	b.d.l.	b.d.l.	b.d.l.	b.d.l.	0.03	b.d.l.	0.02	0.02	b.d.l.	b.d.l.	b.d.l.	b.d.l.	b.d.l.	0.04	b.d.l.	b.d.l.	b.d.l.
FeO	9.52	9.55	9.69	9.69	9.73	9.65	9.69	8.98	8.41	9.57	9.40	9.98	9.65	9.22	9.47	8.48	8.56	8.71	9.52	9.59	8.66	8.81	8.79	8.68	8.76
MnO	0.15	0.18	0.18	0.12	0.17	0.15	0.17	0.12	0.17	0.13	0.16	0.12	0.11	0.15	0.15	0.13	0.12	0.14	0.16	0.16	0.17	0.18	0.16	0.18	0.17
ZnO	0.02	0.05	b.d.l.	b.d.l.	b.d.l.	0.02	b.d.l.	0.04	0.03	b.d.l.	b.d.l.	0.05	0.08	b.d.l.	0.02	b.d.l.	0.03	b.d.l.	0.04	b.d.l.	b.d.l.	0.03	b.d.l.	b.d.l.	0.03
MgO	48.67	48.71	48.55	48.33	48.70	48.62	48.42	49.97	49.90	49.29	49.08	48.93	48.98	49.48	49.33	49.83	49.84	49.83	48.93	49.09	49.70	49.74	49.59	49.53	49.46
NiO	0.33	0.34	0.37	0.34	0.32	0.29	0.34	0.26	0.29	0.34	0.32	0.19	0.26	0.38	0.37	0.37	0.38	0.36	0.35	0.33	0.38	0.37	0.38	0.38	0.42
CaO	b.d.l.	b.d.l.	b.d.l.	b.d.l.	b.d.l.	b.d.l.	b.d.l.	b.d.l.	0.04	b.d.l.	b.d.l.	b.d.l.	0.03	b.d.l.	b.d.l.	b.d.l.	b.d.l.	b.d.l.	b.d.l.	b.d.l.	b.d.l.	0.02	b.d.l.	b.d.l.	0.02
Na_2O	b.d.l.	b.d.l.	b.d.l.	b.d.l.	b.d.l.	b.d.l.	b.d.l.	b.d.l.	b.d.l.	b.d.l.	0.02	b.d.l.	b.d.l.	b.d.l.	b.d.l.	b.d.l.	b.d.l.	0.03	b.d.l.	0.02	b.d.l.	b.d.l.	b.d.l.	b.d.l.	b.d.l.
K_2O	b.d.l.	b.d.l.	b.d.l.	b.d.l.	b.d.l.	b.d.l.	b.d.l.	b.d.l.	b.d.l.	b.d.l.	b.d.l.	b.d.l.	b.d.l.	b.d.l.	b.d.l.	b.d.l.	b.d.l.	b.d.l.	b.d.l.	b.d.l.	b.d.l.	b.d.l.	b.d.l.	b.d.l.	b.d.l.
Total	99.46	99.77	100.11	99.36	99.98	99.81	99.78	100.84	100.08	100.29	99.96	100.29	99.87	100.33	99.97	99.94	99.94	100.00	99.98	100.00	100.32	100.17	100.04	100.01	99.89
Mineral	Ol-1	Ol-1	Ol-1	Ol-1	Ol-2	Ol-2	Ol-2	Ol-1	Ol-1	Ol-2	Ol-2	Ol-1	Ol-1	Ol-2	Ol-2	Ol-1	Ol-1	Ol-1	Ol-2	Ol-2	Ol-1	Ol-2	Ol-2	Ol-2	Ol-2
Si (a.p.f.u.)	1.003	1.004	1.010	1.007	1.005	1.007	1.010	1.003	1.003	0.999	1.003	1.002	0.999	1.000	0.994	1.002	1.000	0.998	1.003	0.999	1.006	0.998	1.002	1.005	1.001
Ti	-	0.001	-	0.000	-	0.000	-	-	-	-	-	0.001	-	0.000	-	-	0.000	0.000	-	-	0.000	0.000	-	-	0.001
Al	-	-	-	-	-	-	-	-	-	-	-	-	-	-	-	-	-	-	-	-	-	-	-	-	-
Cr	0.001	-	-	-	-	-	-	0.000	0.000	-	0.000	-	-	0.000	-	-	-	-	-	-	-	-	0.000	-	0.000
V	-	0.000	-	-	-	-	-	-	-	-	-	-	0.001	-	0.000	0.000	-	-	-	-	-	0.001	-	-	-
Fe^{2+}	0.196	0.196	0.198	0.200	0.199	0.198	0.199	0.182	0.171	0.194	0.192	0.204	0.198	0.188	0.182	0.173	0.175	0.173	0.195	0.194	0.176	0.177	0.179	0.177	0.179
Mn	0.003	0.004	0.004	0.003	0.004	0.003	0.003	0.002	0.003	0.003	0.003	0.002	0.002	0.003	0.003	0.003	0.003	0.003	0.003	0.003	0.003	0.004	0.003	0.004	0.004
Zn	0.000	0.001	-	-	-	0.000	-	0.001	0.001	-	-	0.001	0.001	-	0.000	-	0.001	-	0.001	-	-	0.001	-	-	0.000
Mg	1.787	1.783	1.770	1.776	1.779	1.778	1.771	1.803	1.811	1.795	1.791	1.783	1.792	1.798	1.800	1.812	1.813	1.812	1.787	1.793	1.801	1.808	1.804	1.801	1.803
Ni	0.006	0.007	0.007	0.007	0.006	0.006	0.007	0.005	0.006	0.007	0.006	0.004	0.005	0.007	0.007	0.007	0.007	0.007	0.007	0.007	0.007	0.007	0.007	0.007	0.008
Ca	-	-	-	-	-	-	-	-	0.001	-	-	-	0.001	-	-	-	-	-	-	-	-	0.001	-	-	0.000
Na	-	-	-	-	-	-	-	-	-	-	0.001	-	-	-	-	-	-	0.002	-	0.001	-	-	-	-	-
K	-	-	-	-	-	-	-	-	-	-	-	-	-	-	-	-	-	-	-	-	-	-	-	-	-
O=4	-	-	-	-	-	-	-	-	-	-	-	-	-	-	-	-	-	-	-	-	-	-	-	-	-
Fo	0.90	0.90	0.90	0.90	0.90	0.90	0.90	0.91	0.91	0.90	0.91	0.90	0.90	0.91	0.91	0.91	0.91	0.91	0.90	0.90	0.91	0.91	0.91	0.91	0.91

b.d.l. = below detection limit.

Mineral	Amp	Amp	Amp	Amp	Amp	Amp	Amp	Amp	Chl	Chl	Chl	Chl	Chl	Chl	Chl	Chl	Srp	Srp	Srp	Srp	Srp	Srp	Srp	Srp
Locality	Las Palmas			San Pedro		Patio Bonito			Las Palmas				San Pedro		Patio Bonito		Las Palmas				San Pedro		Patio Bonito	
Type of rock	dun	dun	dun	per	per	dun	dun	dun	dun	dun	dun	dun	per	per	chr	per	dun	dun	dun	dun	per	per	dun	dun
Sample	LP-1	LP-1	LP-1	SP-1	SP-1	CO-7	CO-7	CO-7	LP-1	LP-1	LP-7	LP-7	SP-1	SP-1	CO-4	CO-6	LP-7	LP-7	LP-7	LP-7	SP-1	SP-1	CO-7	CO-7
SiO_2 (wt.%)	58.17	57.73	57.68	57.73	57.77	57.61	56.72	58.48	33.62	33.15	32.26	32.38	34.41	34.20	27.91	27.91	35.54	35.15	34.83	35.12	38.87	36.28	36.85	36.15
TiO_2	0.05	0.08	0.05	b.d.l.	b.d.l.	b.d.l.	b.d.l.	0.02	0.06	0.04	0.10	0.09	b.d.l.	b.d.l.	0.07	0.07	b.d.l.	b.d.l.	b.d.l.	b.d.l.	b.d.l.	b.d.l.	b.d.l.	0.04
Al_2O_3	0.22	0.38	0.33	0.36	0.33	0.43	0.49	0.25	14.09	14.59	16.16	16.23	12.75	13.22	22.17	22.17	0.02	b.d.l.	b.d.l.	b.d.l.	b.d.l.	b.d.l.	b.d.l.	b.d.l.
Cr_2O_3	0.02	0.08	0.36	0.05	0.10	0.03	0.07	0.04	2.67	2.15	1.81	1.71	1.71	1.43	1.24	1.24	b.d.l.	0.02	b.d.l.	b.d.l.	b.d.l.	b.d.l.	b.d.l.	b.d.l.
V_2O_3	b.d.l.	b.d.l.	0.02	b.d.l.	b.d.l.	b.d.l.	b.d.l.	0.02	0.05	0.05	0.02	b.d.l.	0.02	0.04	b.d.l.	b.d.l.	b.d.l.	b.d.l.	b.d.l.	b.d.l.	b.d.l.	0.02	b.d.l.	b.d.l.
FeO	1.81	1.98	1.86	1.89	1.68	1.37	1.50	1.28	2.44	2.47	2.56	2.68	2.29	2.35	1.79	1.79	5.92	6.35	6.13	5.66	4.98	5.95	5.66	6.03
MnO	0.09	0.12	0.06	0.11	0.06	0.04	0.03	0.07	0.03	0.02	0.03	0.04	0.02	b.d.l.	b.d.l.	b.d.l.	0.11	0.12	0.13	0.09	0.07	0.07	0.08	0.05
ZnO	0.04	0.02	0.08	b.d.l.	b.d.l.	b.d.l.	0.04	b.d.l.	b.d.l.	b.d.l.	b.d.l.	b.d.l.	b.d.l.	b.d.l.	b.d.l.	b.d.l.	b.d.l.	b.d.l.	0.03	0.02	0.03	b.d.l.	0.04	0.03
MgO	23.36	23.57	23.11	23.44	23.41	23.90	25.00	23.10	33.55	33.13	32.80	32.39	34.21	33.99	33.56	33.56	39.40	40.20	41.37	40.84	39.13	38.82	40.96	40.60
NiO	0.05	0.08	0.07	0.06	0.11	0.12	0.09	0.07	0.13	0.14	0.13	0.15	0.21	0.21	b.d.l.	b.d.l.	0.17	0.20	0.21	0.22	0.13	0.34	0.36	0.35
CaO	12.74	12.27	12.41	11.96	12.88	13.41	12.89	13.43	b.d.l.	0.02	0.03	0.02	b.d.l.	b.d.l.	b.d.l.	b.d.l.	0.05	0.04	0.02	b.d.l.	0.04	0.03	b.d.l.	0.05
Na_2O	0.27	0.34	0.35	1.05	0.49	0.32	0.24	0.22	0.02	b.d.l.	b.d.l.	b.d.l.	0.05	0.04	b.d.l.	b.d.l.	b.d.l.	b.d.l.	0.02	b.d.l.	b.d.l.	0.03	b.d.l.	b.d.l.
K_2O	b.d.l.	b.d.l.	b.d.l.	b.d.l.	b.d.l.	b.d.l.	b.d.l.	b.d.l.	b.d.l.	b.d.l.	b.d.l.	b.d.l.	b.d.l.	b.d.l.	b.d.l.	b.d.l.	b.d.l.	b.d.l.	b.d.l.	b.d.l.	b.d.l.	b.d.l.	b.d.l.	b.d.l.
H_2O	2.18	2.18	2.17	2.18	2.18	2.19	2.18	2.19	12.65	12.54	12.56	12.53	12.56	12.54	12.75	12.75	11.78	11.87	11.94	11.87	12.19	11.85	12.19	12.07
Total	99.01	98.82	98.54	98.85	99.02	99.42	99.25	99.16	99.31	98.31	98.47	98.23	98.24	98.02	99.51	99.51	92.99	93.95	94.70	93.84	95.46	93.40	96.14	95.37
Mineral	Amp	Amp	Amp	Amp	Amp	Amp	Amp	Amp	Chl	Chl	Chl	Chl	Chl	Chl	Chl	Chl	Srp	Srp	Srp	Srp	Srp	Srp	Srp	Srp
Si (a.p.f.u.)	7.997	7.950	7.975	7.954	7.951	7.905	7.807	8.018	6.375	6.341	6.161	6.196	6.573	6.542	5.249	5.249	3.617	3.552	3.498	3.550	3.825	3.672	3.626	3.593
Ti	0.005	0.008	0.005	-	-	-	-	0.002	0.008	0.006	0.014	0.013	-	-	0.010	0.010	-	-	-	-	-	-	-	-
Al	0.036	0.062	0.054	0.058	0.054	0.070	0.079	0.040	3.149	3.289	3.637	3.660	2.871	2.980	4.914	4.914	0.003	-	-	-	-	-	-	-
Cr	0.002	0.008	0.039	0.006	0.011	0.003	0.007	0.004	0.400	0.325	0.273	0.259	0.258	0.217	0.184	0.184	-	0.001	-	-	-	-	-	-
V	-	-	0.002	-	-	-	-	0.002	0.007	0.008	0.004	-	0.003	0.005	-	-	-	-	-	-	-	0.002	-	-
Fe^{3+}	0.020	0.063	0.024	0.071	0.029	0.000	0.000	0.000	0.000	0.000	0.000	0.000	0.000	0.000	0.282	0.282	0.504	0.537	0.515	0.478	0.350	0.504	0.466	0.501
Fe^{2+}	0.188	0.165	0.191	0.147	0.165	0.157	0.173	0.147	0.387	0.395	0.409	0.429	0.366	0.376	0.000	0.000	0.000	0.000	0.000	0.000	0.059	0.000	0.000	0.000
Mn	0.011	0.014	0.007	0.013	0.007	0.004	0.004	0.009	0.005	0.004	0.005	0.006	0.004	-	-	-	0.009	0.010	0.011	0.008	0.006	0.006	0.006	0.005
Zn	0.005	0.002	0.008	-	-	-	0.004	-	-	-	-	-	-	-	-	-	-	-	0.002	0.002	0.002	-	0.003	0.002
Mg	4.787	4.839	4.763	4.814	4.803	4.889	5.130	4.722	9.483	9.448	9.338	9.240	9.743	9.692	9.409	9.409	5.978	6.057	6.194	6.153	5.740	5.857	6.009	6.015
Ni	0.006	0.009	0.007	0.007	0.012	0.013	0.009	0.008	0.020	0.022	0.020	0.023	0.033	0.033	-	-	0.014	0.016	0.017	0.018	0.010	0.028	0.028	0.028
Ca	1.877	1.810	1.838	1.766	1.899	1.971	1.901	1.973	-	0.003	0.005	0.004	-	-	-	-	0.005	0.004	0.003	-	0.004	0.003	-	0.005
Na	0.073	0.091	0.094	0.280	0.129	0.085	0.063	0.057	0.008	-	-	-	0.017	0.013	-	-	-	-	0.004	-	-	0.005	-	-
K	-	-	-	-	-	-	-	-	-	-	-	-	-	-	-	-	-	-	-	-	-	-	-	-
H	2	2	2	2	2	2	2	2	16	16	16	16	16	16	16	16	8	8	8	8	8	8	8	8
O	24	24	24	24	24	24	24	24	36	36	36	36	36	36	36	36	18	18	18	18	18	18	18	18
Mg#	0.962	0.967	0.961	0.970	0.967	0.969	0.967	0.970	0.961	0.960	0.958	0.956	0.964	0.963	1.000	1.000	1.000	1.000	1.000	1.000	0.990	1.000	1.000	1.000

Table 6. Representative electron microprobe analyses of tremolite, chlorite and serpentine in the metaperidotites and chromitites.

http://dx.doi.org/10.18268/BSGM2020v72n3a120620

http://dx.doi.org/10.18268/BSGM2020v72n3a120620

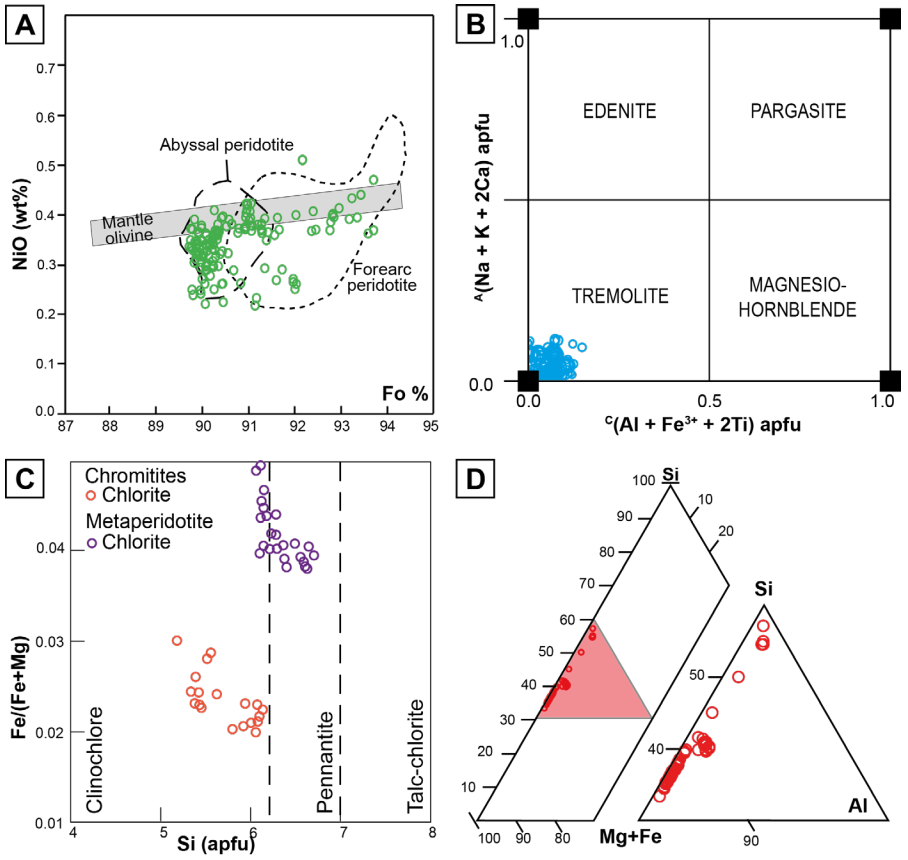

Figure 9 (A) NiO (wt%) vs. Forsterite content (Fo) in olivine from the metaperidotites of the MMU. Fields for mantle olivine are from Takahashi *et al.* (1987), fore-arc peridotite from Ishii *et al.* (1992) and abyssal peridotite from Moghadam *et al.* (2015). (B) Amphibole classification diagram according to Hawthorne *et al.* (2012), variations of ^{A}(Na + K + 2Ca) a.p.f.u. vs. ^{C}(Al + Fe^{3+} + 2Ti) a.p.f.u. (C) Fe/(Fe + Mg) vs. Si a.p.f.u. classification diagram for chlorite according to Hey (1954), for the metaperidotites and chromitites of the MMU. (D) Si, Al, Fe + Mg distribution diagram for serpentine of the MMU metaperidotites.

The MMU protoliths are predominantly harzburgites and dunites with tectonite textures and are similar to abyssal ocean ridge and supra-subduction zone peridotites. The Cr# of the accessory chromian spinel in metaperidotites (0.58 - 0.62, unaltered cores from Type-I chromian spinel) from the MMU overlap those of supra-subduction peridotites from ophiolites (Figure 7A; Pearce *et al.*, 2000; Marchesi *et al.*, 2016 and references therein).

The REE patterns of the studied metaperidotites compare well with those related with supra-subduction zone peridotites (Savov *et al.*, 2005; Marchesi *et al.*, 2006; Deschamps *et al.*, 2010) and differ from those of abyssal peridotites (MOR-type) (Godard *et al.*, 2008), characterized by positive LREE to HREE slopes (Figure 5A). The REE patterns (almost flat or U-shaped) are consistent with melt percolation reactions, common in supra-subduction zones due to volatile-rich fluid infiltration produced by slab dehydration (Proenza *et al.*, 1999; Pearce *et al.*, 2000; Marchesi *et al.*, 2006, 2016). Also, primitive mantle-normalized trace element patterns (Figure 5B) of the studied MMU metaperidotites are similar to supra-subduction zone peridotites from the Tso Morari fore-arc (Savov *et al.*, 2005).

On the other hand, the MMU hosts the major chromian spinel deposits described for Colombia. Several authors have suggested that podiform chromitites are predominantly formed within supra-subduction zone settings (Pearce *et al.*, 1984; Roberts, 1988; Proenza *et al.*, 1999; González-Jiménez *et al.*, 2012, 2014a and references therein). Consequently, the ultramafic rocks in Medellín probably formed in a supra-subduction zone setting, where ophiolites show typical island arc signatures but have oceanic crust structures clearly formed by expansion processes related to a sub-

http://dx.doi.org/10.18268/BSGM2020v72n3a120620

duction zone (*e.g.*,: fore-arc, intra-arc, and back-arc basins). This interpretation agrees with the work by Correa-Martínez (2007), who considers the Aburrá Ophiolite an oceanic back-arc basin formed during the Triassic and later tectonically emplaced during Jurassic time.

5.2. ORIGIN OF THE CHROMIAN SPINEL MINERALIZATION

The studied chromitite samples from Patio Bonito and San Pedro deposits are Al-rich (Figures 7C and 7D) and strongly PGE-depleted (Figure 6). Al-rich chromitites are usually found within the mantle-crust transition zone, or Moho Transition Zone (MTZ), near levels of layered gabbros at the base of the crust in ophiolite complexes (Leblanc and Violette, 1983; Proenza *et al.*, 1999, González-Jiménez *et al.*, 2014a; Mendi *et al.*, 2020). The primary cores of chromian spinel forming the chromitite bodies associated with the MMU exhibit compositions that plot between the fields defined for chromian spinel from mid-ocean ridge basalts (MORB; Dick and Bullen, 1984) and boninite-like lavas (Figure 7D) (Arai, 1992). These compositions are similar to other Al-rich ophiolitic chromitites in central and southern America and the Caribbean region (Figures 7C and 7D) such as Moa-Baracoa, Cuba (Proenza *et al.*, 1999), Tehuitzingo, México (Proenza *et al.*, 2004b), Los Guanacos, Argentina (Proenza *et al.*, 2008), and Cerro Colorado, Venezuela (Mendi *et al.*, 2020).

The composition of the melt in equilibrium with unaltered (magmatic) chromian spinel cores of the Patio Bonito and San Pedro chromitites has been calculated using the following equations (Maurel and Maurel, 1982; Zaccarini *et al.*, 2011):

$$(Al_2O_{3\ melt}) = 4.1386 \cdot \ln (Al_2O_{3\ spinel}) + 2.2828 \quad [1]$$

$$(TiO_{2\ melt}) = 0.708 \cdot \ln (TiO_{2\ spinel}) + 1.6436 \quad [2]$$

$$\ln(FeO/MgO)_{spinel} = 0.47 - 1.07Al\#_{spinel} + 0.64Fe\#_{spinel} + \ln(FeO/MgO)_{melt} \quad [3]$$

The calculations give average values of Al_2O_{3melt} = 15.75 wt%, TiO_{2melt} = 0.41wt% and $(FeO/MgO)_{melt}$ = 0.72 wt%, and plot overlapping the field described for tholeiitic magmas (MORB or BABB) in the FeO/MgO (melt) vs. Al_2O_3 (melt) binary diagram (Figure 10). These types of MORB/BABB magmas are characteristic for back-arc basins, a geodynamic environment consistent with the previously proposed geological setting of the MMU by other authors that is based on the study of the host peridotites (Correa-Martínez, 2007; Restrepo, 2008; García-Casco *et al.*, 2020). The low PGE content in the chromitites is also consistent with the MORB/BABB composition of the parental magmas. PGE content in chromitite is strongly related with the parental magma composition: PGE-rich Cr-rich chromitites usually crystallize from boninitic magmas, whereas PGE-poor Al-rich chromitites (*e.g.*, Colombian chromitites) crystallize from tholeiitic magmas. This is related to the fact that boninitic magmas are S-undersaturated and have higher PGE-contents than tholeiitic magmas, which are S-saturated (Hamlyn *et al.*, 1985; Zhou *et al.*, 1998; González-Jiménez *et al.*, 2014b).

The mechanism of crystallization of the chromitites within the supra-subduction back-arc mantle may be related with the mingling of MORB/BABB melts with different degrees of fractionation within dunite channels (Arai and Yurimoto, 1995; Melcher *et al.*, 1997; Zhou and Robinson, 1997; Proenza *et al.*, 1999, 2004b; González-Jiménez *et al.*, 2011, 2014a). In this model, infiltrating melt reacts with the host harzburgite, generating secondary dunite in equilibrium with a more differentiated MORB/BABB melt, while the necessary Cr for chromitite formation is provided by the dissolution of Cr-rich pyroxene from the host peridotite. Mixing/mingling of melts with different SiO_2 drives supersaturation in Cr in order to crystallize chromian spinel (Arai and Yurimoto, 1995; Melcher *et al.*, 1997), which may be accumulated by bubble flotation in the relatively hydrous melt (Matveev and Ballhaus, 2002), in a self-sustained process to form massive bodies (González-Jiménez *et al.*, 2011, 2014a and references therein).

http://dx.doi.org/10.18268/BSGM2020v72n3a120620

5.3. CHROMIAN SPINEL ALTERATION

Textural and compositional variations observed in the chromian spinel of the MMU cannot be explained by magmatic/metamorphic processes at mantle temperatures or pressures. Instead, these variations suggest an origin related to the post-mantle metamorphic evolution of the ultramafic bodies. The metamorphic mineral associations in the metaperidotites (chlorite + tremolite + talc + forsterite) indicate temperatures of 550-700 ºC, at medium pressures up to 6 kbar (García-Casco *et al.*, 2020).

Compositional and textural variations of the studied chromian spinel could be attributed to cooling associated with a metamorphic cycle during the Permian-Triassic period in the Mesozoic paleomargin of South America. The first transformation of chromian spinel, which forms porous chromian spinel (type II), can be explained by chromian spinel dissolution and chlorite precipitation. Chlorite coronas surrounding chromian spinel and the systematic presence of secondary recrystallized olivine, tremolite and talc indicate medium-T metamorphic imprint (amphibolite facies) during cooling (García-Casco *et al.*, 2020). This transformation is characterized by a decrease in Al and Mg coupled with an increase in Cr and Fe^{2+}. At this stage, the residual chromian spinel is enriched in Cr, whereas the Fe^{3+} content stays invariable. The porous chromian spinel (type II) composition (Mg# vs. TiO_2, MnO, ZnO) is typical of chromian spinel metamorphosed at amphibolite facies (Barnes, 2000; Saumur and Hattori, 2013; Colás *et al.*, 2014, 2019). The formation of this secondary chromian spinel can be represented with the following reaction proposed by González-Jiménez *et al.* (2015):

$$4(Mg_{0.7}Fe_{0.3})CrAlO_4 + 4Mg_2SiO_4 + 2SiO_2(aq.) + 8H_2O \rightarrow 2Mg_5AlSi_3AlO_{10}(OH)_8 + 2(Fe_{0.6}Mg_{0.4})Cr_2O_4 \quad [4]$$

According to these authors, at temperatures between ~ 700 and ~ 400 ºC and in the presence of SiO_2-rich fluids, primary Al-rich chromian spinel reacts with forsterite to produce chlorite and residual porous type II chromian spinel, enriched in Cr and Fe^{2+}.

Homogeneous chromian spinel (type III) is Fe^{3+}-rich in comparison to the other two chromian spinel types (Figure 7B). The Fe^{3+}# values vary from 0.3 to 0.79, and, therefore, this chromian spinel can be classified as ferrian chromian spinel. The formation of ferrian chromian spinel has been interpreted as the reaction product between chromian spinel and secondary magnetite (Barnes, 2000), or between chromian spinel and antigorite (Merlini *et al.*, 2009) during prograde metamorphism. On the other hand, it has also been interpreted as the reaction product between primary chromian spinel and olivine (Gervilla *et al.*, 2012) or between chromian spinel and lizardite (Mellini *et al.*, 2005) during the cooling of an ultramafic body.

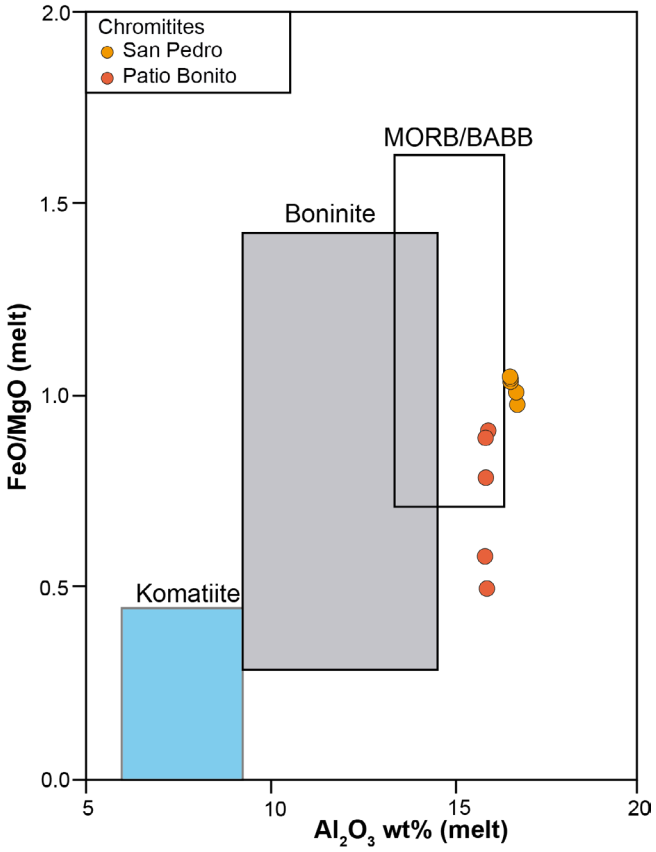

Figure 10 Composition diagram [$(FeO/MgO)_{melt}$ vs. $(Al_2O_3)_{melt}$ (wt%)] of the parental melt in equilibrium with the San Pedro and Patio Bonito chromitites. Melts in equilibrium were calculated using the equations by Maurel and Maurel (1982) and Zaccarini *et al.* (2011). Fields are from Moghadam *et al.* (2015).

http://dx.doi.org/10.18268/BSGM2020v72n3a120620

The homogenous chromian spinel formation implies the dissolution of already formed Cr-rich spinel, probably at oxidizing conditions through the addition of magnetite to the porous Al-Mg-depleted chromian spinel (type II) during a late hydrothermal process starting at temperatures close to 600 ºC and evolving to temperatures lower than 500 ºC (Gervilla *et al.*, 2012) or 350 ºC (Colás *et al.*, 2019). The composition (Mg# vs. TiO_2, MnO, and ZnO) of homogeneous chromian spinel (type III) from the MMU is also typical for metamorphosed chromian spinel in amphibolite facies (Barnes, 2000; Saumur and Hattori, 2013; Colás *et al.*, 2019) with similarities to chromian spinel metamorphosed at greenschist facies.

6. Conclusions

The petrological and geochemical characteristics of the metaperidotites from the MMU indicate that these represent shallow levels of the suboceanic lithospheric mantle related to a supra-subduction zone setting (back-arc basin/incipient arc scenario). The chromian spinel mineralization associated with the MMU is Al-rich (refractory grade) and is strongly depleted in PGE. The most favorable geodynamic setting for such chromitite formation is a back-arc basin, where the chromian spinel crystallizes from a BABB-type tholeiitic magma. Accessory chromian spinel in the metaperidotites is classified as: (i) partially altered chromian spinel with Al-rich cores, (ii) porous Cr-Fe^{2+}-enriched and Al-Mg-depleted chromian spinel, and (iii) homogeneous Fe^{3+}-rich chromian spinel. Textural and compositional variations of accessory chromian spinel in the metaperidotites of the MMU give evidence of the superimposed metamorphic processes of the MMU, which has reached amphibolite facies and later retrograded to the greenschist facies conditions.

Acknowledgements

This research has been financially supported by FEDER Funds and the Spanish Projects CGL2012-36263, CGL2015-65824 and PID2019-105625RB-C21. Fieldwork for sample collection was partly supported the Universidad Nacional de Colombia (project no. 35671) and the Convocatoria para la Movilidad Internacional de la Universidad Nacional de Colombia (project no. 6867). We thank Dr. Antonio García-Casco for his support and feedback during the preparation of this paper. Excellent technical support during EPMA sessions by Dr. X. Llovet and during FESEM sessions by Eva Prats at the Serveis Científics i Tecnòlogics (University of Barcelona) is highly appreciated. Two anonymous reviewers and the special volume editors are profoundly acknowledged for their constructive criticism that has helped to greatly improve the quality of the present manuscript.

References

Álvarez, J., 1987, Mineralogía y química de los depósitos de cromita podiforme de las dunitas de Medellín, Departamento de Antioquia, Colombia: Boletín Geológico Ingeominas, 28, 1-3, 33-46.

Arai, S., Yurimoto, H., 1995, Possible subarc origin of podiform chromitites: The Island Arc, 4(2), 104-111. https://doi.org/10.1111/j.1440-1738.1995.tb00135.x

Arai, S., 1992, Chemistry of chromian spinel in volcanic rocks as a potential guide to magma chemistry: Mineralogical Magazine, 56, 173–184. https://doi.org/10.1180/minmag.1992.056.383.04

Barnes S.J., 2000, Chromite in komatiites, II. Modification during Greenschist to Mid-Amphibolite Facies Metamorphism: Journal of Petrology, 41, 387-409. https://doi.org/10.1093/petrology/41.3.387

Botero-Restrepo, G. 1945. Yacimiento de cromo "El Carmelo" (Municipio de Envigado, Antioquía). CEGOC, Tomo 6, 321-334. Bogotá.

Bourgois, J., Toussaint, J.F., González, H., Azéma, J., Calle, B., Desmet, A., Murcia, L.A., Acevedo, A.P., Parra, E., Tournon, J.,

1987, Geological history of the Cretaceous ophiolitic complexes of northwestern South America (Colombian Andes): Tectonophysics, 143, 307-327. https://doi.org/10.1016/0040-1951(87)90215-0

Case, J.E., Duran S, L.G., Alfonso, L.R., Moore, W.R., 1971, Tectonic investigations in Western Colombia and Eastern Panama: Geological Society of America Bulletin, 82, 2685-2712. https://doi.org/10.1130/0016-7606(1971)82[2685:tiiwca]2.0.co;2

Colás, V., González-Jiménez, J.M., Camprubí, A., Proenza, J.A., Griffin, W.L., Fanlo, I., O'Reilly, S.Y., Gervilla, F., González-Partida, E., 2019, A reappraisal of the metamorphic history of the Tehuitzingo chromitite, Puebla state, Mexico: International Geology Review, 61(14), 1706-1727. https://doi.org/10.1080/00206814.2018.1542633

Colás, V., González-Jiménez, J.M., Griffin, W.L., Fanlo, I., Gervilla, F., O'Reilly, S.Y., Pearson, N.J., Kerestedjian, T., Proenza, J.A., 2014, Fingerprints of metamorphism in chromite: New insights from minor and trace elements: Chemical Geology, 389, 137-152. https://doi.org/10.1016/j.chemgeo.2014.10.001

Correa-Martínez, A.M., Martens, U., 2000, Caracterización geológica de las anfibolitas de los alrededores de Medellín: BS. Thesis, Universidad Nacional de Colombia, Sede Medellín, 363 p.

Correa-Martínez, A.M., Martens, U.C., Restrepo, J.J., Ordoñez-Carmona, O., Pimentel, M., 2005, Subdivisión de las metamorfitas básicas de los alrededores de Medellín – Cordillera Central de Colombia: Revista de la Academia Colombiana de Ciencias Exactas, 29, 112, 325-344.

Correa-Martínez, A.M., Nilson, A., 2003, Dunitas de Medellín y Metagabros de El Picacho: Posibles fragmentos de ofiolita subtipo hartzburgita, tipo zona de suprasubducción (abstract), in IX Congreso Colombiano de Geología: Medellín, 46-47.

Correa-Martínez, A.M., Nilson, A.A., Pimentel, M., 2004, The Aburra Ophiolitic Complex, Antioquia–Colombia a fragment of a harzburgite ophiolite–type in 32nd International Geological Congress: Florence, Italy, Abstracts, 1, p. 374–375.

Correa-Martínez, A.M., 2007, Petrogênese e evolucao do Ofiolito de Aburrá, Cordilhera Central dos Andes Colombianos: PhD. Thesis, Universidade de Brasília, 178 p.

Deschamps, F., Guillot, S., Godard, M., Chauvel, C., Andreani, M., Hattori, K.H., 2010, In situ characterization of serpentinites from forearc mantle wedges: Timing of serpentinization and behavior of fluid-mobile elements in subduction zones: Chemical Geology, 269, 262-277. https://doi.org/10.1016/j.chemgeo.2009.10.002

Dick, H.J.B., Bullen, T., 1984, Chromian spinel as a petrogenetic indicator in abyssal and alpine-type peridotites and spatially associated lavas: Contributions to Mineralogy and Petrology, 86, 54-76. https://doi.org/10.1007/bf00373711

Dilek, Y., Flower, M.F.J., 2003, Arc-trench rollback and forearc accretion: 2. A Model Template for Ophiolites in Albania, Cyprus, and Oman, in Dilek, Y., and Robinson, P.T. (ed.), Ophiolites in Earth history: London, Geological Society (London) Special Publication, 218, 43-68. https://doi.org/10.1144/gsl.sp.2003.218.01.04

Dilek, Y., Furnes, H., 2014, Ophiolites and their Origins: Elements, 10, 2, 93-100. https://doi.org/10.2113/gselements.10.2.93

Feininger, T., Botero, G., 1982, The Antioquian Batholith, Colombia: Publicaciones Especiales Ingeominas, 12, 1-50.

Feininger, T., Barrero, D., Castro, N., 1972, Geología de parte de los departamentos de Antioquia y Caldas (sub-zona II-B): Boletín Geológico Ingeominas. 20, 2, 1-160.

García-Casco, A., Restrepo, J.J., Correa–Martínez, A.M., Blanco–Quintero, I.F., Proenza, J.A., Weber, M., Butjosa, L., 2020. The petrologic nature of the "Medellín Dunite" revisited:

http://dx.doi.org/10.18268/BSGM2020v72n3a120620

An Algebraic Approach and Proposal of a New Definition of the Geological Body, in Gómez, J. and Pinilla–Pachon, A.O. (ed.), The Geology of Colombia, Volume 2 Mesozoic. Servicio Geológico Colombiano, Publicaciones Geológicas Especiales 36, p. Bogotá. https://doi.org/10.32685/pub.esp.36.2019.02

Gervilla, F., Padrón-Navarta, J.A., Kerestedjian, T., Sergeeva, I., González-Jiménez, J.M., Fanlo, I., 2012, Formation of ferrian chromite in podiform chromitites from the Golyamo Kamenyane serpentinite, Eastern Rhodopes, SE Bulgaria: a two-stage process: Contributions to Mineralogy and Petrology, 162, 643-657. https://doi.org/10.1007/s00410-012-0763-3

Gervilla, F., Proenza, J.A., Frei, R., González-Jiménez, J.M., Garrido, C.J., Melgarejo, J.C., Meibom, A., Díaz-Martínez, R., Lavaut, W., 2005, Distribution of platinum-Group elements and Os isotopes in chromite ores from Mayarí-Baracoa Ophiolitic Belt (eastern Cuba): Contributions to Mineralogy and Petrology, 150, 589-607. https://doi.org/10.1007/s00410-005-0039-2

Godard, M., Lagabrielle, Y., Alard, O., Harvey, J., 2008, Geochemistry of the highly depleted peridotites drilled at ODP Sites 1272 and 1274 (Fifteen-Twenty Fracture Zone, Mid-Atlantic Ridge): Implications for mantle dynamics beneath a slow spreading ridge: Earth and Planetary Science Letters, 267, 410-425. https://doi.org/10.1016/j.epsl.2007.11.058

Gómez, J., Montes, N.E., Nivia, Á., Diederix, H., compiladores., 2015, Mapa Geológico de Colombia 2015. Escala 1:1 000 000. Servicio Geológico Colombiano, 2 hojas. Bogotá.

González-Jiménez, J.M., Griffin, W.L., Gervilla, F., Proenza, J.A., O'Reilly, S.Y., Pearson, N.J., 2014b, Chromitites in ophiolites: How, where, when, why? Part I. A review and new ideas on the origin and significance of platinum-group minerals: Lithos, 189, 127-139. https://doi.org/10.1016/j.lithos.2013.06.016

González-Jiménez, J.M., Griffin, W.L., Proenza, J.A., Gervilla, F., O'Reilly, S.Y., Akbulut, M., Pearson, N.J., Arai, S., 2014a, Chromitites in ophiolites: How, where, when, why? Part II. The crystallization of chromitites: Lithos, 189, 140-158. https://doi.org/10.1016/j.lithos.2013.09.008

González-Jiménez., J.M., Augé, T., Gervilla, F., Bailly, L., Proenza, J.A. and Griffin, W.L., 2012, Mineralogy and geochemistry of platinum-rich chromitites from the mantle-crust transition zone at Ouen Island, New Caledonia ophiolite: The Canadian Mineralogist, 49, 1549-1570. https://doi.org/10.3749/canmin.49.6.1549

González-Jiménez, J.M., Reich, M., Camprubí, A., Gervilla, F., Griffin, W.L., Colás, V., O'Reilly, S.Y., Proenza, J.A., Pearson, N.J., Centeno-García, E., 2015, Thermal metamorphism of mantle chromites and the stability of noble-metal nanoparticles: Contributions to Mineralogy and Petrology, 170(2), 15. https://doi.org/10.1007/s00410-015-1169-9

Hall, R.B., Feininger, T., Barrero, D., Rico, H., Alvarez, J., 1970, Recursos minerales de parte de los departamentos de Antioquia y Caldas: Boletín Geológico Ingeominas, 18 (2), 1-90.

Hamlyn, P.R., Keays, R.R., Cameron, W.E., Crawford, A.J., Waldron, H.M., 1985, Precious metals in magnesian low-Ti lavas: implication for metallogenesis and sulfur saturation in primary magmas: Geochimica et Cosmochimica Acta, 49, 1797-1811. https://doi.org/10.1016/0016-7037(85)90150-4

Hawthorne, F.C., Oberti, R., Harlow, G.E., Maresch, W.V., Martin, R.F., Schumacher, J.C., Welch, M.D., 2012, Nomenclature of the amphibole supergroup: American Mineralogist, 97(11-12), 2031-2048. https://doi.org/10.2138/am.2012.4276

Hey, M.H., 1954, A new revision of the chlorite: Mineralogical Magazine, 30, 277-292.

Irvine, T.N., 1967, Chromian spinel as a petrogenetic indicator: Part II. Petrologic

applications: Canadian Journal of Earth Sciences, 4, 71-103. https://doi.org/10.1139/e67-004

Ishii, T., Robinson, P.T., Maekawa, H., Fiske, R., 1992, Petrological studies of peridotites from diapiric serpentinite seamounts in the Izu-Ogasawara-Mariana forearc, Leg 125, in Fryer, P., Pearce, J.A., Stokking, L.B., et al. (ed.), Proceedings of the Ocean Drilling Program, Scientific Results, College Station,TX: Ocean Drilling Program, 125, 445-485. https://doi.org/10.2973/odp.proc.sr.125.129.1992

Kamenetsky, V.S., Crawford, A.J., Meffre, S., 2001, Factors Controlling Chemistry of Magmatic Spinel: an Empirical Study of Associated Olivine, Cr-spinel and Melt Inclusions from Primitive Rocks: Journal of Petrology, 42, 655-671. https://doi.org/10.1093/petrology/42.4.655

Kerr, A.C., Tarney, J., Marriner, G.F., Nivia, A., Klaver, G.T.,, Saunders, A.D., 1996, The geochemistry and tectonic setting of late Cretaceous Caribbean and Colombian volcanism: Journal of South American Earth Sciences, 9, 1-2, 111-120. https://doi.org/10.1016/0895-9811(96)00031-4

Lázaro, C., García-Casco, A., Blanco-Quintero, I.F., Rojas-Agramonte, Y., Corsini, M., Proenza, J.A., 2014, Did the Turonian–Coniacian plume pulse trigger subduction initiation in the Northern Caribbean? Constraints from $^{40}Ar/^{39}Ar$ dating of the Moa-Baracoa metamorphic sole (eastern Cuba): International Geology Review, 57, 919-942. https://doi.org/10.1080/00206814.2014.924037

Leblanc, M., Nicolas, A., 1992, Les chromitites ophiolitiques: Chronique de la Recherche Minière, 507, 3–25.

Leblanc, M., Violette, J.F., 1983, Distribution of aluminium-rich and chromium-rich chromite pods in ophiolite peridotites: Economic Geology, 78, 293-301. https://doi.org/10.2113/gsecongeo.78.2.293

Leblanc, M., 1991, Platinum-group elements and gold in ophiolitic complexes: distribution and fractionation from mantle to oceanic floor, in Peters, T.J., Nicolas, A., Coleman, R.G. (ed.), Ophiolite Genesis and Evolution of Oceanic Lithosphere, Dordrecht, Kluwer Academic Publisher, 231-260. https://doi.org/10.1007/978-94-011-3358-6_13

Locock, A.J., 2014, An Excel spreadsheet to classify chemical analyses of amphiboles following the IMA 2012 recommendations: Computers & Geosciences, 62, 1-11. https://doi.org/10.1016/j.cageo.2013.09.011

López, M.C., Moreno-Sánchez, M., Audemard, F.A., 2009, Deformación tectónica reciente en los piedemontes de las Cordilleras Central y Occidental, Valle del Cauca, Colombia: Boletín de Geología, 31, 11-29.

Marchesi, C., Garrido, C.J., Godard, M., Proenza, J.A., Gervilla, F., Blanco-Moreno, J., 2006, Petrogenesis of highly depleted peridotites and gabbroic rocks from the Mayarí-Baracoa Ophiolitic Belt (eastern Cuba): Contributions to Mineralogy Petrology, 151, 717-736. https://doi.org/10.1007/s00410-006-0089-0

Marchesi, C., Garrido, C.J., Proenza, J.A., Hidas, K., Varas-Reus, M.I., Butjosa, L., Lewis, J.F., 2016, Geochemical record of subduction initiation in the sub-arc mantle: Insights from the Loma Caribe peridotite (Dominican Republic): Lithos, 252, 1-15. https://doi.org/10.1016/j.lithos.2016.02.009

Marchesi, C., Jolly, W.T., Lewis, J.F., Garrido, C.J., Fernandez, J.P., Lidiak, E.G., 2011, Petrogenesis of fertile mantle peridotites from the Monte del Estado massif (Southwest Puerto Rico): a preserved section of Proto-Caribbean lithospheric mantle?: Geologica Acta, 9(3-4), 289-306. https://doi.org/10.1344/105.000001713

Matveev, S., Ballhaus, C., 2002, Role of water in the origin of podiform chromitite deposits: Earth and Planetary Science Letters, 203, 235-243. https://doi.org/10.1016/s0012-821x(02)00860-9

http://dx.doi.org/10.18268/BSGM2020v72n3a120620

Maurel, C., Maurel, P., 1982, Etude expérimentale de la distribution de l'aluminium entre bain silicaté basique et spinelle chromifère. Implications pétrogénétiques: teneur en chrome des spinelles: Bulletin Minéralogie, 105, 197-202. https://doi.org/10.3406/bulmi.1982.7605

Maya, M., González, H., 1995, Unidades litodémicas en la Cordillera Central de Colombia: Boletín Geológico Ingeominas, 35, 23, 43-57.

McCourt, W.J., Aspden, J.A., Brook, M., 1984, New geological and geochronological data from the Colombian Andes: continental growth by multiple accretion: Journal of the Geological Society, 141, 831-845. https://doi.org/10.1144/gsjgs.141.5.0831

McDonough, W.F. and Sun, S.S., 1995, The composition of the Earth: Chemical Geology, 120, 223-253. https://doi.org/10.1016/0009-2541(94)00140-4

Melcher, F., Grum, W., Grigore, S., Thalhammer, V.T., Stumpfl, E.F., 1997, Petrogenesis of the Ophiolitic Giant Chromite Deposits of Kempirsai, Kazakhstan: a study of solid and fluid inclusions in chromite: Journal of Petrology, 38, 1419-1458. https://doi.org/10.1093/petroj/38.10.1419

Mellini M., Rumori C., Viti, C., 2005, Hydrothermally reset magmatic spinels in retrograde serpentinites: formation of "ferritchromit" rims and chlorite aureoles: Contributions to Mineralogy Petrology, 149, 266-275. https://doi.org/10.1007/s00410-005-0654-y

Mendi, D.J., González-Jiménez, J.M., Proenza, J.A., Urbani, F., Gervilla, F., 2020, Petrogenesis of the chromitite body from the Cerro Colorado ophiolite, Paraguaná Peninsula, Venezuela: Boletín de la Sociedad Geológica Mexicana, 72(3), A280719. http://dx.doi.org/10.18268/BSGM2020v72n3a280719

Merlini A., Grieco G. and Diella, V., 2009, Ferritchromite and chromian-chlorite formation in mélange-hosted Kalkan chromitite (Southern Urals, Russia): American Mineralogist, 94, 1459-1467. https://doi.org/10.2138/am.2009.3082

Moghadam, H.S., Khedr, M.Z., Arai, S., Stern, R., Ghorbani, G., Tamura, A. and Ottley, C.J., 2015, Arc-related harzburgite–dunite–chromitite complexes in the mantle section of the Sabzevar ophiolite, Iran: A model for formation of podiform chromitites: Gondwana Research, 27, 575-593. https://doi.org/10.1016/j.gr.2013.09.007

Moreno-Sánchez, M., Pardo-Trujillo, A., 2003, Stratigraphical and sedimentological constrains on western Colombia: implications on the evolution of the Caribbean Plate, in Bartolini, C., Buffler, R.T., Blickwede, J.F. (eds.), The Circum-Gulf of Mexico and the Caribbean: hydrocarbon habitats, basin formation, and plate tectonics: American Association of Petroleum Geologist, 79, 891-924.

Naldrett, A.J., Duke, J.M., 1980, Platinum metals in magmatic sulfide ore: Science, 280, 117-1428. https://doi.org/10.1126/science.208.4451.1417

Nivia, A., 1987, The geochemistry and origin of the Amaime and Volcanic sequences, SW Colombia, MSc. Thesis, University of Leicester, Unpublished, 164 p.

Nivia, A., 1993, Evidencias de obducción en el Complejo Ultramáfico de Bolívar, in VI Congreso Colombiano de Geología, 63-79.

Nivia, A., 1996, The Bolivar mafic-ultramafic complex, SW Colombia: the base of an obducted oceanic plateau: Journal of South American Earth Sciences, 9, 59-68. https://doi.org/10.1016/0895-9811(96)00027-2

Nivia, A., 2001, Mapa Geológico del Departamento del Valle, Escala 1:250.000: Memoria Explicativa, Ingeominas, 148.

Pearce, J.A., Barker, P.F., Edwards, S.J., Parkinson, I.J., Leat, P.T., 2000, Geochemistry and tectonic significance of peridotites from the South Sandwich arc-basin system, South Atlantic: Contributions to Mineralogy

and Petrology, 139, 36-53. https://doi.org/10.1007/s004100050572

Pearce, J.A., Lippard, S.J., Roberts, S., 1984, Characteristics and tectonic significance of suprasubduction zone ophiolites, in Kokelaar, B.P., y Howells, M.F. (ed.), Marginal Basin Geology: Geological Society, London Special Publication, 16, 77-94. https://doi.org/10.1144/gsl.sp.1984.016.01.06

Pereira, E., Ortiz, F., Prichard, H., 2006, Contribución al conocimiento de las anfibolitas y dunitas de Medellín (Complejo Ofiolítico de Aburrá): Dyna, 149, 17-30.

Proenza, J.A., Escayola, M., Ortiz, F., Pereira, E., Correa-Martínez, A.M., 2004a, Dunite and associated chromitites from Medellín (Colombia) (abstract), in 32nd International Geological Congress: Florencia, Italia.

Proenza, J.A., Gervilla, F., Melgarejo, J.C., Bodinier, J.L., 1999, Al- and Cr- rich chromitites from the Mayarí-Baracoa Ophiolitic Belt (eastern Cuba): consequence of interaction between volatile-rich melts and peridotite in suprasubduction mantle: Economic Geology 94, 547-566. https://doi.org/10.2113/gsecongeo.94.4.547

Proenza, J.A., Ortega-Gutiérrez, F., Camprubí, A., Tritlla, J., Elías-Herrera, M., Reyes-Salas, M., 2004b, Paleozoic serpentinite-enclosed chromitites from Tehuitzingo, (Acatlán Complex, southern Mexico): a petrological and mineralogical study: Journal of South American Earth Sciences, 16, 649-666. https://doi.org/10.1016/j.jsames.2003.12.003

Proenza, J.A., Zaccarini, F., Escayola, M., Cábana, C., Shalamuk, A., Garuti, G., 2008, Composition and textures of chromite and platinum-group minerals in chromitites of the western ophiolitic belt from Córdoba Pampeans Ranges, Argentine: Ore Geology Reviews, 33, 32-48. https://doi.org/10.1016/j.oregeorev.2006.05.009

Restrepo, J.J., Toussaint, J.F., 1973, Obducción cretácea en el Occidente Colombiano: Publicación Especial de Geología, 3, 1-26.

Restrepo, J.J., Toussaint, J.F., 1984, Unidades litológicas de los alrededores de Medellín, in I Conferencia sobre riesgos geológicos del Valle de Aburrá, Medellín: Sociedad Colombiana de Geología, Memoria, 1, 1-26.

Restrepo, J.J., 1986, Metamorfismo en el sector norte de la Cordillera Central de Colombia: Universidad Nacional de Colombia Sede Medellín, Informe para promoción,276.

Restrepo, J.J., 2008, Obducción y metamorfismo de las ofiolitas triásicas en el flanco occidental del Terreno Tahamí, Cordillera Central de Colombia: Boletín Ciencias de la Tierra, 22, 49-100.

Roberts, S., 1988, Ophiolitic chromitite formation: a marginal basin phenomenon?: Economic Geology, 83, 1034-1036. https://doi.org/10.2113/gsecongeo.83.5.1034

Rodríguez, G., González, H., Zapata, G., Cossio, U., Correa-Martínez, A.M., 2016. Geología de la Plancha 147 Medellín Oriental, Escala 1:50.000, versión 2016: Memorias. Servicio Geológico Colombiano, Medellín, 464 p.

Saumur, B.M., Hattori, K.H., 2013, Zoned Cr-spinel in forearc serpentinites along the northern Caribbean Margin, Dominican Republic: Mineralogical Magazine, 77, 117-136. https://doi.org/10.1180/minmag.2013.077.1.11

Savov, I.P., Ryan, J.G., D'Antonio, M., Kelley, K., Mattie, P., 2005, Geochemistry of serpentinized peridotites from the Mariana Forearc Conical Seamount, ODP Leg 125: implications for the elemental recycling at subduction zones: Geochemistry, Geophysics, Geosystems, 6, 4, 1-24. https://doi.org/10.1029/2004gc000777

Serrano, L.M., 2009, Origen de la isla Gorgona (Colombia) y su relación con el Plateau del Caribe: MSc. Thesis, Universidad Nacional Autónoma de México, 135 p.

Spikings, R., Paul, A., 2019, The Permian – Triassic history of magmatic rocks of the northern Andes (Colombia and Ecuador): Supercontinent assembly and disassembly, in Gómez, J. and Pinilla–Pachon, A.O.

http://dx.doi.org/10.18268/BSGM2020v72n3a120620

(ed.), The Geology of Colombia, Vol. 2 Mesozoic. Servicio Geológico Colombiano: Publicaciones Geológicas Especiales 36, 42 p. Bogotá. https://doi.org/10.32685/pub.esp.36.2019.01

Takahashi, E., Uto, K., Schilling, J.G., 1987, Primary magma compositions and Mg/Fe ratios of their mantle residues along Mid-Atlantic Ridge 29N to 73N: Technical Reports Institute for Study of the Earth's Interior Okayama University Ser APY, 9, 1-14.

Vinasco, C., 2019, The Romeral Shear Zone, in Cediel F., Shaw, R.P., (Ed.) Geology and Tectonics of Northwestern South America: The Pacific-Caribbean-Andean Junction, Frontiers in Earth Sciences, Switzerland, Springer, 833-876. https://doi.org/10.1007/978-3-319-76132-9_12

Vinasco, C.J., Cordani, U.G., González, H., Weber, M., Pelaez, C., 2006, Geochronological, isotopic, and geochemical data from Permo-Triassic granitic gneisses and granitoids of the Colombian Central Andes: Journal of South American Earth Sciences, 21(4), 355-371. https://doi.org/10.1016/j.jsames.2006.07.007

Zaccarini, F., Garuti, G., Proenza, J.A., Campos, L., Thalhammer, O.A.R., Aiglsperger, T., Lewis, J., 2011, Chromite and platinum-group-elements mineralization in the Santa Elena ophiolitic ultramafic nappe (Costa Rica): geodynamic implications: Geologica Acta, 9, 407-423.

Zhou, M.F., Robinson, P.T., 1997, Origin and tectonic environment of podiform chromite deposits: Economic Geology, 92, 259-262. https://doi.org/10.2113/gsecongeo.92.2.259

Zhou, M.F., Sun, M., Keays, R.R., Kerrich, R.W., 1998, Controls on platinum-group elemental distributions of podiform chromitites: A case study of high-Cr and high-Al chromitites from Chinese orogenic belts: Geochimica et Cosmochimica Acta, 62, 677-688. https://doi.org/10.1016/s0016-7037(97)00382-7